APPLICATION OF DENSITY FUNCTIONAL THEORY TO PROPYLENE TO PROPYLENE OXIDE CATALYTIC REACTION

A THESIS SUBMITTED TO
THE GRADUATE SCHOOL OF NATURAL AND APPLIED SCIENCES
OF
MIDDLE EAST TECHNICAL UNIVERSITY

BY

DENİZ ONAY

IN PARTIAL FULFILLMENT OF THE REQUIREMENTS
FOR
THE DEGREE OF MASTER OF SCIENCE
IN
CHEMICAL ENGINEERING

FEBRUARY 2012

Approval of the thesis:

APPLICATION OF DENSITY FUNCTIONAL THEORY TO PROPYLENE TO PROPYLENE OXIDE CATALYTIC REACTION

submitted by **DENİZ ONAY** in partial fulfillment of the requirements for the degree of **Master of Science in Chemical Enginnering Department, Middle East Technical University** by,

Prof. Dr. Canan Özgen _____
Dean, Graduate School of **Natural and Applied Sciences**

Prof. Dr. Deniz Üner _____
Head of Department, **Chemical Engineering**

Prof. Dr. Işık Önal _____
Supervisor, **Chemical Engineering Dept., METU**

Assist. Prof. Dr. Mehmet Ferdi Fellah _____
Co-Supervisor, **Chemical Engineering Dept., Yüzüncü Yıl University**

Examining Committee Members

Prof. Dr. İnci Eroğlu _____
Chemical Engineering Dept., METU

Prof. Dr. Işık Önal _____
Chemical Engineering Dept., METU

Assoc. Prof. Dr. Görkem Külah _____
Chemical Engineering Dept., METU

Assist. Prof. Dr. Mehmet Ferdi Fellah _____
Chemical Engineering Dept., Yüzüncü Yıl University

Dr. Derya Düzenli _____
Maden Analizleri ve Teknolojisi, MTA

Date: 16.02.2012

I hereby declare that all information in this document has been obtained and presented in accordance with academic rules and ethical conduct. I also declare that, as required by these rules and conduct, I have fully cited and referenced all material and results that are not original to this work.

Name, Surname: Deniz Onay

Signature:

ABSTRACT

APPLICATION OF DENSITY FUNCTIONAL THEORY TO PROPYLENE TO PROPYLENE OXIDE CATALYTIC REACTION

Onay, Deniz

M.S., Department of Chemical Engineering

Supervisor : Prof. Dr. Işık Önal

Co-Supervisor: Assist. Prof. Dr. Mehmet Ferdi Fellah

February 2012, 95 pages

Current propylene oxide production highly relies on costly and environmentally disadvantageous processes. Direct propylene epoxidation on heterogeneous surface is desired to replace these processes. With this ultimate goal in mind, propylene epoxidation has been investigated on $Cu_2O(001)$ and $RuO_2(110)$ surfaces. Different elementary steps of the reaction mechanism that result in propylene oxide formation are analyzed on these catalytic models by using Density Functional Theory (DFT) calculations via Vienna Ab initio Simulation Package (VASP). CI-NEB method is utilized for the activation barrier analysis. Beside propylene oxide, formations of side products, such as allyl radical, acrolein, acetone and propionaldehyde, are also examined in order compare the activity of the surfaces.

Two different mechanisms that lead to propylene oxide are distinguished on the surfaces, namely 'surface intermediate type mechanism' and 'direct

mechanism'. For both of the mechanisms, $Cu_2O(001)$ surface, which is covered with oxygen, is found to be ineffective for formation of propylene oxide. Rather than propylene oxide, allyl radical which finally results in acrolein is favored over this surface.

Both type of mechanisms are investigated on two different type of $RuO_2(110)$ surfaces, namely '$RuO_2(110)$ surface' and 'RuO_2-O_γ surface', the latter is modeled by the consideration of oxygenated reaction medium. Surface intermediate type mechanism is found to result in a blocking effect for formation of any of the products on $RuO_2(110)$ surface. Unlike $RuO_2(110)$ surface, both mechanisms are favored for propylene oxide formation on RuO_2-O_γ surface as a result of the higher activity of O_γ species which is also found to be the most electrophilic oxygen species in this study.

Keywords: Propylene, epoxidation, Density Functional Theory, ruthenium oxide, copper oxide

ÖZ

YOĞUNLUK FONSİYONELİ TEORİSİNİN PROPİLENDEN PROPİLEN OKSİT KATALİTİK TEPKİMESİNE UYGULANMASI

Onay, Deniz

Yüksek Lisans, Kimya Mühendisliği Bölümü

Tez Yöneticisi : Prof. Dr. Işık Önal

Ortak Tez Yöneticisi : Yrd. Doç. Dr. Mehmet Ferdi Fellah

Şubat 2012, 95 sayfa

Günümüzdeki propilen oksit üretimi maliyeti yüksek ve çevreye zararlı proseslere dayalıdır. Bu proseslerin yerine geçebilmesi için heterojen yüzey üzerinde doğrudan propilen epoksidasyonunun sağlanması istenmektedir. Bu nihai hedefi düşünerek, $Cu_2O(001)$ ve $RuO_2(110)$ yüzeyleri üzerinde propilen epoksidaysonu incelenmiştir. Propilen oksit oluşumu ile sonuçlanan farklı reaksiyon mekanizma basamaklarının elemanları, bu katalitik modeller üzerinde Yoğunluk Fonksiyoneli Teorisi (YFT) hesaplamaları kullanılarak Vienna Ab initio Simulasyon Paketi (VASP) ile analiz edilmiştir. Aktivasyon bariyeri analizi için CI-NEB metodu kullanılmıştır. Propilen oksit oluşumunun yanısıra, allil radikali, akrolein, aseton ve propiyonaldehit gibi yan ürünlerin oluşumları da yüzeylerin aktifliğini karşılaştırabilmek amacı ile incelenmiştir.

Yüzeyler üzerinde propilen oksit oluşumunu sağlayan, 'yüzey ara ürünü tipli mekanizma' ve 'direk mekanizma' olarak adlandırılan iki farklı mekanizma bulunmuştur. Üst yüzeyi oksijen ile kaplı olan $Cu_2O(001)$ yüzeyi, her iki mekanizma tipi için de propilen oksit oluşumu için etkisiz olarak bulunmuştur. Propilen oksit yerine, akrolein oluşumu ile sonlanan alil radikali oluşumunu tercih etmektedir.

Her iki mekanizma, $RuO_2(110)$ yüzeyine ait, '$RuO_2(110)$' ve 'RuO_2-O_Y' yüzeyi olarak adlandırılan, iki farklı tip yüzey üzerinde incelenmiştir, bunlardan ikincisi oksijen içeren reaksiyon ortamını düşünerek modellenmiştir. Yüzey ara ürünü tipli mekanizmanın, $RuO_2(110)$ yüzeyi üzerinde oluşabilecek ürünler üzerinde bloke edici etkiye sahip olduğu bulunmuştur. $RuO_2(110)$ yüzeyi ile karşılaştırılınca, mekanizmaların her ikisinin de RuO_2-O_Y yüzeyi üzerinde tercih edilen mekanizmalar olduğu açığa çıkmıştır. Aktif olan O_Y türü, bu çalışmada yer alan katalitik yüzeyler üzerindeki oksijenler arasında en yüksek elektrofilik özelliğe sahiptir.

Anahtar Kelimeler: Propilen, epoksidasyon, Yoğunluk Fonsiyoneli Teorisi, ruthenyum oksit, bakır oksit.

To my family

ACKNOWLEDGEMENT

I am very grateful to my supervisor Prof. Dr. Işık Önal who gave me the all possibility to complete this thesis. I would like to thank Mr. Önal for giving valuable comments and encouragement through my student life. It has been always an honor for me to study with him.

I would like to thank to Dr. Mehmet Ferdi Fellah for his valuable comments and guidance; Dr. M. Oluş Özbek for his teachings, great supports and friendship throughout the study; Dr. Derya Düzenli for her support; Emine Kurnaz for her friendship, support and understanding. I also want to thank Pelin Yetişemiyen, Miray Gülbiter, Duygu Gerçeker, Merve Çınar, Eda Açık, Saygın Aras for their support.

I particularly want to thank Serkan Balaban for always being ready to encourage and support even in the tough times. I am also grateful to my dear friend Pervin Gizem Gezer for all the times that have been shared and that are to be shared in our invaluable friendship. I would like to express special thanks to Selin Noyan and Nagehan Keskin for their encouragement and support. I would like to thank specially to Merve Savaşlıoğlu and Şafak Temel who have motivated me fully in all our conversations. I want to thank Ceren Tüfekçi and Selçuk Doğan for their kindness and hospitality. Thanks to Tülay and Serkan Topçuoğlu for their great friendship.

Furthermore, I want to acknowledge my family members for their endless confidence in me. I appreciate my dear mum and dad; Sevim Onay and Süleyman Onay, I always feel your caring and trust. I would like to thank to my sister Pınar Onay Durdu and my brother Levent Durdu, for all the encouragement and support that you provided. I also want to share my

deepest feelings to my dearest new-born nephew İdil Durdu. I am very grateful to have such a great family that has an endless encouragement and love.

Finally, I would like to express my endless appreciation to Volkan Atmaca, for his endless support and understanding throughout all the time we spend together. Thank you so much for your belief in me and for being in my life.

TABLE OF CONTENTS

LIST OF TABLES

TABLES

LIST OF FIGURES

FIGURES

CHAPTER 1

INTRODUCTION

The purpose of this study is to understand the epoxidation behavior of propylene molecule on $Cu_2O(001)$ and $RuO_2(110)$ catalytic oxide surfaces and to investigate underlying factors that has influence on the epoxidation mechanism. Density Functional Theory (DFT) is implemented to analyze the reaction mechanism on these catalytic surfaces. Introductory information is gathered for both propylene oxide formation and catalytic approach. Finally a brief introduction is presented for the analysis tool of the study, which is DFT.

1.1. Background of the Study

Background of the study is introduced firstly in the epoxides point of view. Propylene epoxidation is the first contributor of the study. In the corresponding introduction part, the details of the epoxidation lead to the need for a heterogeneous catalytic surface. Understanding the reactivity of the catalytic surfaces is crucial for achieving the ultimate goal of discovering a viable catalyst. Therefore an introductory part is given also for general explanation of the catalytic point of view which can be referred as another contributor of the study.

1.1.1. Epoxides Point of View

As a versatile intermediate, epoxides are valuable materials in chemical industry. Epoxides are used both as an end-product and an intermediate. Epoxidation is the partial oxidation of a selected alkene to form the epoxide. During epoxidation an oxidant is required to achieve the cyclic epoxide bond with three ring atoms.

Among the epoxides, ethylene oxide and propylene oxide are the major commodity chemicals. Ethylene glycol, nonionic alkyl-phenol ethoxylates which are surface-active agents are produced via ethylene oxide. Besides, there are many fine petroleum and chemical intermediates and derivatives of ethylene oxide (EO) which are used in several industries such as electronics, pharmaceuticals, pesticides, textiles, papermaking, automobiles, oil recovery and oil refining. Polyurethane polyols, propylene glycols, P-series glycol ethers, di- and tri- propylene glycols, polyalkylene glycols, allyl alcohol, isopropylamines are produced via propylene oxide (PO). These chemicals are used in applications such as, textile, construction, drugs, cosmetics, solvents, plasticizers, heat transfer and hydraulic fluids, antifreezes, sterilization of packaged foods, pesticides [1].

Production of EO is based on direct oxidation of ethylene with air or oxygen in a packed bed, recycled multi-tubular reactor with the use of silver catalyst supported on α-Al_2O_3 where promoters are also included. Heterogeneous epoxidation of ethylene is enabled by direct silver catalyzed heterogeneous partial oxidation in large scale, whereas propylene, which is a higher order alkene, it cannot be achieved yet.

Propylene oxide production requires several indirect steps as seen in Figure 1.1. Chlorine reacts with water to form chlorohydrin as the product in

chlorohydrin process. Then, PO is formed with the reaction of chlorohydrin with a base such as calcium hydroxide. By-product of this reaction, calcium chloride is to be removed as disposal. Half of the worldwide production of propylene oxide mainly relies on chlorohydrin process. However, this process produces environmentally disadvantageous co-products.

Another production method for propylene oxide is epoxidation with organic hydroperoxides which can be the products of isobutene, ethylbenzene and cumene oxidation reaction. During hydroperoxide processes, co-products are produced more than the amount of propylene oxide. Therefore, as an ultimate production step, propylene oxide is to be removed from the crude mixture of propylene oxide.

Both of the processes for PO production, chlorohydrin and hydroperoxide, are costly disadvantageous since they require complex facilities. Instead of these processes, simpler method has been developed for propylene epoxidation with the use of hydrogen peroxide. However, this reaction requires substantial production of H_2O_2 capacity. Due to the stoichiometry, 1 kg of H_2O_2 is needed for production of 1.7 kg of propylene. [2]. Thus, utilization of hydrogen peroxide for formation of propylene oxide is not a sustainable manufacturing method.

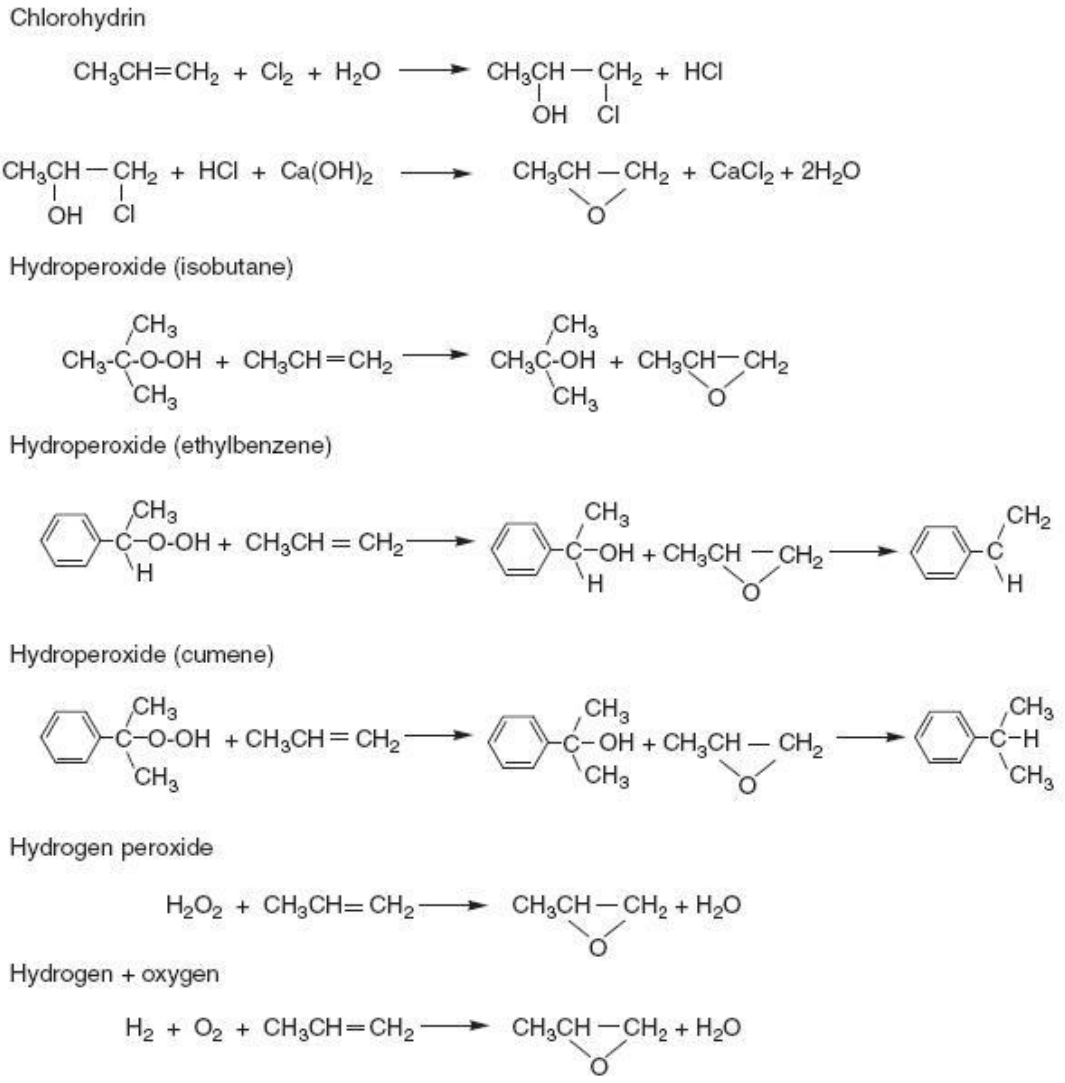

Figure 1.1: Propylene oxide production technologies [1]

As can be inferred, it would be advantageous to find a direct and selective path for propylene oxide production to overcome current difficulties in all current production techniques. Using only molecular oxygen on a catalytic surface, similar to current ethylene oxide production on silver catalyst, is the promising process that can be proposed for production of propylene oxide.

1.1.2. Catalytic Point of View

The importance of catalysis is far beyond dispute since it is used in extensive fields that are crucial for human beings. Catalysts are used for their ability to facilitate the adsorption of reactants and their conversion into products. Production of foods, car fuels, purification technologies and many goods that we commonly consume, even the biological transformations in human body, take the advantage of the catalytic activity. Basically catalyst is a material that should have high activity to produce only the desired product selectively for prolonged periods of time [3].

Catalytic reactions proceeds through five main steps namely, chemisorption, dissociation (activation), diffusion, recombination and desorption. These steps follow each other in a cyclic manner. During chemisorption, reactants or intermediates are adsorbed on the catalytic surface. This has an influence on the bond-weakening of the reactants for achieving a transition to form the products. Desorption of the product creates an empty site on the catalytic surface and completes the catalytic cycle. Following that, a new cycle begins by the adsorption of the reactants. If the adsorption of the reactants and the catalyst is too strong, desorption of the final product from the surface becomes harder. To put it differently, highest reaction rate is achieved if reactants and catalyst interacts at an optimum value in terms of adsorption. This is known as Sabatier principle [3].

Transition state theory defines unstable intermediates as transition states of the reactions. These structures are observed during formation of products from reactants and they define the catalytic behavior. Reactant and the transition state are assumed to be in equilibrium with the transition state complex. Rate limiting step is said to be the number of molecules in the transition state that leads to formation of the product [4]. Transition state

theory divides the elementary step of a reaction into two regions namely, the reactant region and the product region. Transition state (TS) is the border between two areas. In both regions there are lowest energy configurations, namely initial state (IS) and final state (FS) [5].

In addition to adsorption strength of the reactants as stated previously during explanation of Sabatier principle, prediction of the elementary steps is also required to endeavor the analysis of the catalytic activity. Equilibrium thermodynamics which consists of enthalpy of the reaction and free energy; and non-equilibrium thermodynamics which consists of activation energy and activation entropy are related with Bronsted-Evans-Polanyi (BEP) relation. During reaction mechanism, if the transition state is close to reactants, it is called early transition state; in the same manner when transition state is close to products, it is called late transition state. If reaction is through early transition state, change of reaction enthalpy, variations of the catalysts do not affect the reaction rate at high levels. However, for late transition state observation, the rate of reaction is highly affected by variations of the catalyst and reaction energy has strong influence on the reaction rate. When there is a tight contact with the surface, transition state entropy for a surface reaction is found to be small. Conversely, when the reactants are desorbed from the surface changes of the activation entropies are larger for elementary steps of the reaction mechanism [3].

For the analysis of catalytic activity, structure of the catalysis and composition also play an important role. When the coordinative unsaturation of the surface metal atoms increases, adsorption energy becomes higher. In other words, if the atoms share fewer bonds with different adsorbates, chemical bond strength increases. If the surface of the catalyst is covered closely by the surface atoms, reactivity of the catalyst becomes less. Moreover, presence of steps or kink sites on the catalyst has also influence

on the catalytic activity. Size of the catalyst particles also introduces unique behavior to the catalyst, especially when the size is less than a critical value. Furthermore, concentration of the adsorbates has the tendency to alter surface construction. Reconstruction may result in more active catalytic surface [3].

To summarize, catalytic activity is a complex function of the contributions from activation energy of the rate determining step, adsorption/desorption enthalpies of the reactant/product and the fractional occupancies of the catalytic surface. Finally size and shape of the catalyst has also strong effect on the catalytic activity.

Besides the concept of catalytic activity, selectivity is also an important attribute of the catalysts. Transformation of the reactant may result in formation of different products. Selective catalyst for a specific reaction is the one that results in the desired product [6].

In consequence, for the effective analysis in the search of a viable catalyst, it is firstly required to examine elementary reactions in terms of catalytic activity and selectivity.

1.2. Analysis Tool of the Study : Density Functional Theory (DFT)

There are various experimental techniques for the analysis of catalytic reactivity that is employed for many different catalytic reactions. Beside these methods, utilization of theoretical calculations that are based on quantum chemical technique has become common for understanding the behavior of catalysts beginning from the molecular level. Therefore catalytic systems are modeled in order to analyze the reactivity of bond breaking and making steps by employing quantum-mechanical methods that represents

real catalytic models. Density functional theoretical calculations on successfully modeled systems stand for ultra high vacuum (UHV) conditions. These calculations, when compared with experimental studies, are within the engineering accuracy of 5 kj/mol. It is possible to measure catalytic reactivity through 3 main approaches in terms of active sites. These approaches are named as; cluster, embedded cluster and periodic methods. Cluster approach presents only a local region that is formed by discrete numbers of atoms. Embedded cluster approach includes several clusters where they are inserted in the subsequent model. Periodic approach is defined by a proper unit cell where it is enlarged in x,y and z directions [3].

All the approaches of the quantum chemical calculations are based on the electron assembly phenomena since they are the building block of physical properties of the molecules. Hence, electronic distributions and interactions should be covered. These terms are included in the Schrödinger's equation:

$$\hat{H}\psi = E\psi \qquad (1.1)$$

$\hat{H}$ is Hamilton operator for a molecular system with M nuclei and N electrons and it includes kinetic and potential contributions of both. Since, masses of nuclei and electrons are different, the latter is lighter; movement of the nuclei is much slower than the electrons. Due to this reason, Born-Oppenheimer or clamped nuclei approximation simplifies Schrödinger's equation by neglecting the kinetic energy of the nuclei. Besides, potential energy due to nucleus-nucleus repulsion is a constant. Ψ is the wave function that defines the state of the system by using 3N spatial coordinates ($\vec{r}_i$), N spin coordinates ($\vec{s}_i$) of the electrons. All the information about a quantum system is gathered within the wave function. Numerical value of the energy of the state is shown with term E.

Wave function based quantum chemical methods mainly uses Hartree-Fock (HF) approximation. HF methodology includes movements of electrons in the field of the nuclei, whereas it does not describe breakings of the bonds. Complete Active Space Self-Consistent Field (CASSCF) procedure covers the correlation of active space and the inactive molecular orbitals considering different configurations. The configuration of active orbitals introduces a challenge to the methodology. Therefore dynamical correlations are brought together to present correction to the energy and the wavefunction.

Definition of electron energy of the systems by their electron density is indicated by Hohenberg-Kohn theorems. Hartree-Fock methods rely on approximate solutions of Schrödinger equation to have multielectron wavefunction and it does not include electron density. However, according to Hohenberg-Kohn theorems, ground state electron density of the system determines the ground state of the system with electrons, or in other words wavefunction of the system. Ground state energy has kinetic and potential energy terms. These terms are function of electron density. By keeping the nuclei fixed; kinetic energy term is the sum of kinetic energy of the electrons, potential energy term is the interaction of electron-nuclei and electron-electron. All these terms are function of ground state densities. Electron density for minimizing the total energy is found when the external potential field is kept fixed. Minimum value of the energy is found for ground state density of the corresponding external potential, yet it is hard to find the ground state wavefunction of the corresponding ground state density. Kohn and Sham presented a model for the local potential. Local potential consists of interacting electrons together with noninteracting electron system. Hence, exchange-correlation energy term is introduced. In order to find the exact value of the exchange-correlation energy, there is a requirement to make approximations. Local density approximation (LDA) gives too large bond

energies since it includes the assumption of uniform electron density within the local system. Generalized gradient approximation is a more sophisticated tool, because beside local density, gradients are also included [7].

DFT is applicable to periodical systems which are formed of repetitive units throughout the space defined along the lattice vectors. Kohn-Sham equation becomes equal to the multiplication of periodic part of the cell and plane wave-like modulation. There is also the concept of k vector which is the band index for different solutions of Schrödinger equation. Vector k is within the Brillouin zone of the reciprocal space. It is necessary to perform integrations over Brillouin zone for finding charge density, density of states and the total energy of the system. Infinite number of k-points is necessary to find charge density directly. Instead of applying uncertain amount of k-points, approximations that involve sum of discrete k-points are used since close k-points are nearly same. Monkhorst-Pack method is used for sampling the Brillouin zone by (n_1xn_2xn_3) grids in reciprocal space.

Electronic wavefunctions are expanded to the plane wave basis sets. However, description of tightly bound states and rapid oscillations of the wavefunctions which are close to nucleus cannot be defined easily. Therefore approximations are used, namely frozen core and pseudopotential approximation. Valence electrons determine the most of the physical properties of the materials whereas; core electrons are far from the real environment. According to frozen core approximation, core electrons are kept fixed in order to reduce the amount of wavefunctions that requires to be solved.

Pseudopotential approximation utilizes a selection of an effective one that stands for plane wave basis sets accordingly. It is selected when the

scattering properties of the wavefunction is the same with the real ionic potential upon true valence wavefunction.

PAW method is one of the pseudopotential approximations that are widely used. All electron wavefunctions of total energies and forces are within the framework of PAW method. This method introduces highly accurate results which are in agreement with experimental results.

There are also hybrid functionals that also accounts for nonlocal Hartree-Fock exchange to the corresponding density functional. Among the hybrid functional, PBE0, HSE03 and B3LYP are the different types of construction schemes.

1.3. Objectives of the Study

Propylene oxide is a valuable commodity that is used in many industries. Up to date, propylene oxide formation is mainly based on economically and environmentally disadvantageous processes. Heterogeneously catalyzed epoxidation of propylene is proposed as a solution to avoid disadvantages of current manufacturing techniques. However, a viable catalyst has not been discovered that produces propylene oxide selectively with high activity. This study mainly aims to find out a catalytic surface that is selective and active for propylene epoxidation. Instead of performing experimental studies, DFT methods are employed to model the catalytic surfaces for investigation of the entire propylene epoxidation mechanism which is also in the need to be enlightened. DFT calculations enable highly detailed molecular analysis in the catalytic point of view. Therefore, a guide to further studies for propylene epoxidation catalytic mechanism is also to be presented throughout the study.

CHAPTER 2

LITERATURE SURVEY

There are extensive research studies which are in the effort to find a viable heterogeneous catalyst which successfully achieves production of propylene oxide directly by using molecular oxygen. In addition to these studies, the mechanism of propylene epoxidation is also under investigation to consolidate the knowledge further for the development of an effective catalyst. The phenomenon of propylene epoxidation presents unknown catalyst together with unknown mechanism which is needed to be discovered by researchers.

2.1. Propylene Epoxidation Catalysts

Extensive efforts have been put forward by researchers to find a viable catalyst for heterogeneous propylene epoxidation on different catalysts and catalyst couples.

Monodispersed silver clusters were prepared by an arc cluster ion source and analyzed via grazing incidence small angle x-ray scattering (GISAXS) and SEM for their size and shape during epoxidation reaction. Particle size remained same (23.1±0.5 nm) after the reaction. Shapes of the clusters were affected when propylene was introduced into the reaction medium. Catalytic activity of the clusters was shifted from formation of acrolein to

formation of propylene oxide when temperature increased from 50°C to 80°C. Morphological changes of the clusters were claimed to the possible factor for different product formations [8].

Besides monodispersed silver clusters, Ag nanoparticles on alumina support had also been investigated for propylene epoxidation by a combined experimental and theoretical study. Silver particles with 3.5 nm size were placed on the support confirmed by grazing incidence small-angle x-ray scattering (GISAXS) at 110°C. Propylene oxide, acrolein and carbon dioxide were the main products. It was found out that selectivity toward propylene oxide was higher at temperatures up to 120°C. Moreover DFT results where Ag_3 nanoparticles are placed on alumina support verified the experimental results by presenting a low barrier during the mechanism of propylene oxide formation [9].

Following the study of Ag_3 nanoparticles on alumina surface, propylene oxide and acrolein formations were compared on silver catalysts with different size to point out to the size dependency of the catalytic reaction. Smaller clusters, at 8.7 and 12 nm, prepared on alumina support were concluded to lead to acrolein formation whereas larger silver clusters at 23.3 nm are found to exhibit propylene oxide formation [10].

Au surface, where oxygen was deposited on, was studied experimentally for epoxidation of propylene. Whereas, it was claimed that acrolein was the main product instead of propylene oxide on the catalytic Au surface. Using isotope of hydrogen inside the propylene molecule presented small amount of propylene oxide where C-H activation by oxygen was not observed on the surface. So that this study suggested modification of the properties of oxygen on Au surface was to be produce desired epoxidation products. The

study proposed change of acidic or basic character of the oxygen on the surface [11].

Au (111) surface, where atomic oxygen was placed on hcp hollow site of the slab, was also investigated via a DFT study which confirmed the finding of inefficiency of Au surface toward catalytic propylene oxide formation. Relative energy profile was investigated for both OMMP surface intermediate and allyl radicals. The energy barrier for OMMP formation was found to be higher than allyl radical formation [12].

Different cluster models of both Ag and Au with 5 and 7 atoms were also studied by a DFT study where propylene epoxidation reaction is compared with ethylene epoxidation reaction where silver is the well-known catalytic surface. Anionic, neutral and cationic models were also analyzed for the reactions. Throughout the findings, only cationic Au_7 cluster was found to favor propylene oxide formation towards pi-allyl formation [13].

By using high-throughput pulsed laser ablation (HT-PLA) technique, 35 different metal catalysts on SiO_2 support had been examined in array channel micro-reactors which enable screening of the catalysts rapidly. Highest amount of PO was formed on Cr, Mn, Cu, Ru, Pd, Ag and Sn metal catalysts on SiO_2 support. This result verified the activity of Cu, Pd and Ag and also demonstrated new metal leads for PO formation. To achieve both higher propylene conversion and PO selectivity, Kahn and his co-workers focused on Mn and Cu bimetallic catalyst on SiO_2 support. Cu-on-Mn/SiO_2 catalyst functioned better than both uni-metallic systems. Moreover, Mn-on-Cu/SiO_2 worked best for PO synthesis indicating that order of deposition was also crucial [14].

Despite the demanding efforts of researchers, catalyst that is effective for obtaining propylene oxide from propylene has not been discovered yet.

2.1.1. Copper Catalysts

Copper is one of the most common catalysts that have been investigated for propylene epoxidation. The oxidation state of copper during propylene epoxidation is a controversial issue in literature. It is still unknown whether metallic or oxide form of copper is responsible for propylene epoxidation.

Vaughan and co-workers studied on Cu/Silica catalysts which are reduced by H_2 during catalyst preparation. During reaction, promoters or hydrogen co-feed were not introduced. Highest propylene selectivity was observed at 225°C. At elevated temperatures formations of acrolein and CO_x increased. They state that active phase for epoxidation to propylene oxide was highly dispersed Cu^0 species which was able to survive at lower temperature regimes [15].

Cu/SiO_2 catalyst was analyzed by FT-IR spectroscopy for CO and C_3H_6 coadsorption on Cu^0, Cu^+ and Cu^{2+} to gather information on activation of propylene by different valance states of Cu species. It was found that C_3H_6 could strongly bond to Cu^0 and Cu^+ sites; however it adsorbed weakly on Cu^{2+}. Reaction results revealed that both Cu^0 and Cu^+ species favored propylene epoxidation and Cu^{2+} species produced acrolein instead of propylene oxide. Activation of C=C bond, which is the required step for propylene oxide formation, was greater on Cu^0 species when compared with C^+ species [16].

Butadiene, which is a higher olefin, was investigated for epoxidation of higher order olefins on Cu/SiO_2 catalyst. By X-ray diffraction and XPS, it was presented that under the reaction conditions the catalyst was in oxide form rather than metallic form [17]. To determine the oxidation state of copper in working catalyst, FT-IR studies combined with XRD measurements was

conducted. It was concluded that for propylene epoxidation Cu (I) was the active site [18].

XPS measurements of another study on Cu/SiO_2 catalyst indicated presence of isolated-like ionic Cu^{2+} species at low metal loading. At higher metal loadings of Cu/SiO_2 catalyst, both Cu^{2+} species and Cu species existing in the isolated-like ionic form had been identified [19].

$VCe_{1-x}Cu_x$ catalyst with NaCl modification was investigated for propylene epoxidation with H_2 co-feed to reaction medium for the stability of the operation by keeping Cu species in its low valance. Cu and NaCl containing catalyst resulted in acrolein formation with 73.6% selectivity. It is considered that copper become cuprous oxide during the reaction. Highest PO selectivity was observed on $VCe_{0.2}Cu_{0.8}$-NaCl(20) catalyst. It is stated that reduced Cu species is responsible for formation of PO [20].

Cuprous and cupric oxide have been investigated by core level XPS, resonant photoemission and temperature-programmed desorption for partial oxidation of propylene to acrolein mechanism. It was found that reactivity of cupric oxide toward propylene oxidation was greater than cuprous oxide. The reactivity of CuO surface was mainly for formation of nonselective highly oxidized products. The mechanism of propylene to acrolein started with initial H atom abstraction which is followed by insertion of oxygen rapidly. Formation of alkoxide surface intermediate decomposed more rapidly on cuprous oxide surface involving hydride elimination to form acrolein as the product [21].

CuO_x/SBA-15 catalyst was studied with K^+ modification and without any reductive treatments. Catalyst was pretreated with O_2 containing flow. This indicates that copper of the catalyst was in oxide form. Catalyst characterization revealed that copper species are mainly Cu(II)O clusters and

isolated Cu(II) ions. When catalyst was not modified with K^+, acrolein formation was the governing product. K^+ modification resulted in PO formation as the main partial oxidation product. K^+ modified oxidized state of copper was found to be responsible for PO formation [22].

Promoting effect of K^+ modification to CuO_x/SBA15 catalyst was found to be in relation with the inhibiting effect of K^+ on reactivity of nucleophilic oxygen species which are in fact lattice oxygen. The lattice oxygen was concluded to be responsible for acrolein formation instead of propylene oxide formation. Also it was concluded as strength and amount of Lewis acid sites of the catalyst are decreased by K^+ modification [23].

Unsupported copper catalyst with VO_x modification was used for distinguishing active sites for PO formation mechanism. It was observed that PO was formed at lower temperatures with less than 0.2% conversion without VO_x modification. Main product was acrolein. When temperature was increased, selectivity of acrolein and PO both decreased. However, VO_x modification resulted in PO as the main partial oxidation product with conversion of 2.7% and selectivity of 16%. XRD measurements of the study revealed that after the introduction of reactant gas during reaction conditions, diffraction peaks of metallic copper decreased and cubic Cu_2O peaks were observed. Cubic Cu_2O was observed to be the main phase in the working VO_x-Cu catalyst. XPS characterization verified that Cu^I functioned for epoxidation of C_3H_6 by O_2 instead of Cu^0 state. Reactivity of the lattice oxygen of Cu_2O was examined. Due to the nucleophilic character of the lattice oxygen, it mainly catalyzed the allylic oxidation of propylene to acrolein. Reactivity of the lattice oxygen of Cu_2O was found to decrease after VO_x modification which results in PO formation instead of acrolein formation [24].

Copper oxide obviously proposes a complicated scheme for the investigation of propylene epoxidation. Oxidation state of the copper is not clear in literature throughout the mechanism of propylene epoxidation. Even the efficiency of the copper oxide species is not clear towards formation of propylene oxide. These results are driving factors for this study to make analysis on oxide form of copper.

2.1.2. Ruthenium Catalysts

Another focus catalyst of this study is ruthenium oxide. Propylene epoxidation mechanism on ruthenium oxide catalyst is to be investigated. But before that, ruthenium and ruthenium oxide studies are searched throughout the literature in general.

Other than propylene epoxidation, $RuO_2(110)$ surface was investigated for both selective oxidation of methanol and ethylene by a DFT study application to slabs through VASP code. Methanol oxidation to formaldehyde was controlled thermodynamically, since relative adsorption energy of the reactants was higher than the partially oxidized CH_3OH. RuO_2 surface was concluded to be selective to formaldehyde formation. On the contrary, ethylene epoxide was thermodynamically hindered as a result of higher adsorption energy of the products which would remain on the surface for further oxidation. Formation of ethylene oxide was also kinetically blocked on RuO_2 surface due to the diffusion of O_{cus} species on the surface [25].

Ethylene epoxidation was also studied on stoichiometric and oxygen rich $RuO_2(110)$ surface by using thermal desorption spectroscopy (TDS) and high-resolution energy-loss spectroscopy (HREELS). After the exposure of $RuO_2(110)$ surface with oxygen, electrophilic oxygen species, O_{cus}, had been generated by dissociative adsorption where O_2 requires two neighboring

sites. Ethylene adsorption is followed by the reaction where π-bonding (-C=O) was shifted to σ-bonding (-C-O). Dehydrogenation step included formation of H_2O on Ru_{cus}. Rate of reaction was highest at Ru_{cus} and O_{cus} neighboring sites. Formation of ethylene oxide was not detected in any cases due to protruding of O_{cus} out of the surface [26].

Trimetallic catalyst of RuO_2-CuO_x-NaCl/SiO_2 was observed to show PO selectivity of 40-50% at propylene conversions of 10-20%. This study was performed at 240-270°C and atmospheric pressure. Single and binary metal combinations did not show good epoxidation performances. It was suggested that when Ru is combined with NaCl, it provides low basicity of CuO_x sites. This effect of NaCl leaded to harder abstraction of allylic hydrogen. Moreover NaCl could result in finely adjusted adsorption sites which are thermally stable. Powder X-ray diffraction showed distinct phases of RuO_2, CuO and NaCl. RuO_2 crystals were demonstrated to exhibit crystals of tetragonal rutile structure [27].

Ru-Cu (111) bimetallic catalyst was investigated in comparison with Cu (111) catalyst by using periodic DFT calculations. One monolayer of copper atoms was modeled on top of Ru (0001) surface resulting in four atomic layers. Previous studies were confirmed by the finding of Cu (111) surface favoring oxametellacycle formation instead of stripping of allylic hydrogen. Ru-Cu(111) surface was came out to be a poor model for propylene epoxidation since it favored stripping of hydrogen atom. Furthermore effect of the basicity of the surface oxygen on propylene epoxidation was validated. Because Ru-Cu(111) surface had an oxygen with higher basicity when compared with Cu(111) surface. This finding is consistent with the fact that lower basicity of surface oxygen is responsible for epoxide formation [28].

Ruthenium based catalysts are being used effectively for investigation in many other oxidation reactions as a model. Activity of ruthenium oxide is not clear towards formation of propylene oxide.

2.2. Propylene Epoxidation Mechanism

Besides a viable catalyst has not been discovered for propylene epoxidation, the mechanism for the formation of propylene oxide on the catalytic surface has not been identified clearly up to now.

Mechanism for epoxidation on heterogeneous surface is still waiting to be revealed even for lighter alkenes. Heterogeneous epoxidation of ethylene on silver catalyst is an industrial process. Although ethylene epoxidation is a common process, the mechanism that leads to ethylene oxide is still ambiguous. During ethylene oxide production, formation of a surface intermediate called oxametallacycle was suggested by investigation through high resolution electron energy loss spectroscopy (HREELS) and density functional theory (DFT). The oxametallacycle surface intermediate contains O-C-C backbone that is bound to the catalytic surface at both ends [29]. In a recent DFT study, on Ag_2O (001) surface oxametallacycle formation was not observed during ethylene oxide formation. Instead of surface intermediate formation, it was pointed out direct exothermic pathway without activation barrier was followed for epoxidation [30]. In the same manner with ethylene epoxidation, mechanism that leads to propylene oxide on heterogeneous catalyst is still unknown.

Analogous oxametallacycle surface intermediate (OMMP) was proposed for propylene epoxidation. Ag (111) and Cu (111) catalytic surfaces were investigated by DFT for propylene epoxidation. Oxygen adatoms were located at three fold sites of the metal surfaces. Basicity of surface oxygen

atom was found responsible for allylic hydrogen stripping which is the competing reaction with OMMP formation. Cu (111) surface was identified to favor propylene epoxidation when compared with Ag (111) due to the presence of lower basicity of oxygen on copper [31].

In addition to unexplored epoxidation mechanism that has been mentioned before, it should also be noted that propylene is a higher alkene which contains allylic hydrogen group. Presence of allylic hydrogens introduces complexity to the phenomena of propylene epoxidation mechanism.

Silver and copper catalysts were also compared experimentally in terms of reaction mechanism by using allylbenzene, α-methylstyrene and trans-methylstryene. These are used as mimic for propylene since all of them contain allylic hydrogen atoms. Ag surface only catalyzed burning of the alkenes whereas copper behaved as a potential epoxidation catalyst. Cu was more selective than Ag in the presence of allylic H atoms containing catalysts. It was also revealed that proximity of C=C bond to the metal surface played a key role for epoxidation mechanism [32].

Allylbenzene (AB), α-methylstyrene (α-MS) and trans-methylstryene (TMS) were explored on Cu surface for their effectiveness in the epoxidation with respect to their adsorption geometries. Cu surface was found to be effective for α-MS and TMS, whereas for epoxidation of AB Cu was inert. The reason for this is their different adsorption geometries on Cu surface. α-MS and TMS adsorbed on the surface with planar geometry where their vinyl group and allylic H atoms were close to the surface. Since C=C bond of α-MS was closest to the surface, it gave highest epoxidation selectivity. For the case of AB, C=C group was directed away from the surface which verified inert behavior of AB for epoxidation [33].

TMS was investigated on Cu catalyst to understand the epoxidation mechanism. TMS and oxygen are dosed to the surface for both dosing order; TMS first, oxygen second and vice versa. When oxygen was dosed first, selectivity of epoxidation was lower. This showed that formation of oxidic islands on the surface did not function as epoxidation catalyst. Cropley and his co-workers also confirmed that allylic hydrogen abstraction suppressed formation of epoxidation products by formation of strongly adsorbed entities that ended up combustion [34].

These studies, investigated throughout the literature, clearly indicate the uncertainty of the reaction mechanism steps that enable formation of propylene oxide.

CHAPTER 3

COMPUTATIONAL METHODOLOGY

This chapter firstly presents the calculation strategy throughout the study to achieve the purpose of investigating the propylene epoxidation mechanism. Furthermore, $Cu_2O(001)$ and $RuO_2(100)$ catalytic surfaces are presented starting from the literature information gathered related with their surface structure. After gaining insight on the surface models, constructions of the slabs are given in detail. Finally, each step for the analysis of reaction mechanism is identified.

3.1. Calculation Strategy for VASP Software

Vienna Ab initio Simulation Package (VASP) is utilized for Density Functional Theory (DFT) calculations [35, 36]. Systems are modeled periodically by using supercell approach and plane wave basis sets [36]. PW basis sets with generalized gradient approximation (GGA) have been utilized [37, 38]. Descriptions of core electrons are obtained by Projected Augmented Wave (PAW) method [39]. The results of all calculations are relaxed until the net forces acting on atoms are smaller than 0.015 eV/Å. The energy cut off is 500 eV. Since asymmetric slabs are used for calculations, standard dipole corrections are included for the removal of dipole moment [35]. 4x4x1 k-point Monkhorst-Pack mesh are used for description of the reciprocal space of the supercells [40].

Relative energy profile that leads to analysis of transition state for each reaction throughout the reaction mechanism is investigated. Climbing Image-Nudged Elastic Band (CI-NEB) method is utilized to find saddle points in the minimum energy path [41]. Firstly initial and final state geometries are optimized, and then CI-NEB method utilization enables analysis of activation barriers between two geometries for each step in the mechanism. By the help of vibrational frequency analysis, transition states of all steps are characterized with Hessian matrix calculations of finite difference approach within step size distance of 0.02 Å along each direction.

Calculation strategy followed throughout the study begins with bulk structure preparation and optimization. Next, slab that represents the catalytic surface of $Cu_2O(001)$ and $RuO_2(110)$ has been prepared and optimized. Firstly, reactants are optimized in vacuum before the calculations on catalytic surfaces. After modeling surface intermediates and products, their energies are all calculated on these well optimized slabs analogously. Finally activation barrier analysis has been performed between initial and final geometries of each mechanism steps.

3.2. Copper Oxide Surface Model

Presence of oxygen in the propylene epoxidation medium underlines the fact that copper would possibly be oxidized to copper oxide species. Copper has two different oxidation states, namely cuprous and cupric oxide, Cu_2O and CuO respectively. This study focuses on Cu_2O surface. Structure of Cu_2O surface is searched throughout the literature.

Ultraviolet photoelectron spectroscopes (UPS) and low energy electron diffraction (LEED) studies were conducted to investigate geometric and electronic structure of oxygen dosed Cu_2O single-crystal surfaces. Ordered,

reconstructed Cu-terminated surface and O-terminated polar $Cu_2O(100)$ surface were formed by ion bombardment and vacuum annealing [42].

$Cu_2O(100)$ surface was analyzed with DFT based calculations and ab-initio thermodynamics approach for understanding the structure and also investigating CO oxidation on the surface. O-terminated surface was found to be more favorable when compared to Cu-terminated $Cu_2O(100)$ surface. When CO reached to the oxygen species on the surface, CO_2 molecule was formed and desorbed spontaneously. Desorption of CO_2 resulted in O-vacancy on the surface. Further calculations revealed that dissociative adsorption of oxygen species present in the gas phase resulted in restoration of the surface [43].

Gathering information on the structure of $Cu_2O(001)$ surface, FCC crystallized cuprite structure with space group of Fm-3m and space number of 225, is obtained with lattice bulk constants a=4.30 Å. (15x15x15) k-points and 500 eV cut-off energy are used for calculation of lattice parameters to optimize the bulk structure. 15 Å vacuum thickness is added in z-direction to eliminate the physical interaction of periodic models in z-direction. Supercell of 2x2 $Cu_2O(001)$ surface that enables enough surface area for the examination of movement of reactants and products is obtained. Top and side views of optimized $Cu_2O(001)$ surface is shown in Figure 3.1 (a) and (b) respectively. Copper atoms present at the bottom are kept fixed in x,y and z directions. Remaining of the slab is kept relaxed throughout the calculations.

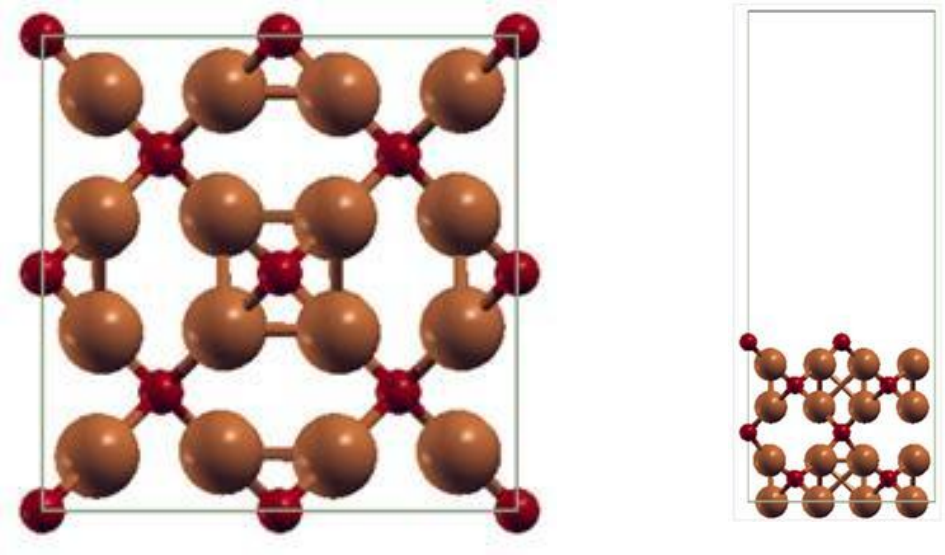

(a) Top view (b) Side view

Figure 3.1: Optimized $Cu_2O(001)$ surface where smaller red atoms represent oxygen atoms and bigger brown atoms represent copper atoms

3.3. Ruthenium Oxide Surface Model

In order to model heterogeneously catalytic surface of ruthenium oxide, reactivity and structure of oxide phase of ruthenium is investigated throughout the literature. Firstly it is found that reactivity of $RuO_2(110)$ is under investigation for many different reactions. Secondly, formation of the $RuO_2(110)$ surface in terms of presence of different oxygen species is being observed in many studies.

During chemical reactions it was revealed that $RuO_2(110)$ surface restored its structure continuously due to interplay of different oxygen atoms on the surface. Low-energy electron diffraction (LEED) and high-resolution electron

loss spectroscopy (HREELS) studies indicates that treatment of Ru(0001) surface with $1x10^7$ langmuirs of oxygen at 700K, leaded to $RuO_2(110)$ surface. Exposure of further oxygen to $RuO_2(110)$ surface resulted in weakly held oxygen atoms (O_γ). The study verified the presence of weakly held oxygen species on top of the Ru_{cus} sites of the surface. It was also argued that O_γ atoms possibly represents electrophilic nature due to charge cloud around O_γ species according to density difference plots of the DFT study [44].

Reactivity of $RuO_2(110)$ catalyst was also investigated for catalytic oxidation of ammonia selectively to either N_2 or NO. Catalytically active site of the surface was verified as coordinatively unsaturated ruthenium (Ru_{cus}) species of the surface on which ammonia or oxygen is adsorbed. Selective oxidation of ammonia was determined according to concentration of oxygen atoms adsorbed on the reactive site [45].

In addition to ammonia oxidation, NO_x adsorption and reactions was also analyzed on $RuO_2(110)$ surface by DFT calculations with supercell approach. It was shown that instead of oxidation or decomposition, NO species are effectively adsorbed on RuO_2 [46].

Besides chemical reactions on $RuO_2(110)$ surface, analysis about the structure of the $RuO_2(110)$ surface in the literature has guided this study thoroughly. After treatment of high doses of O_2, Ru(0001) surface was observed to form well ordered structure of RuO_2 (110) surface which was also confirmed by LEED analysis. Scanning tunneling microscopy (STM) and DFT analysis of the study revealed the structure of the atoms which were present on RuO_2 (110) surface model along [001] direction. Bridging oxygen atoms (O_{br}) were present at the topmost plane of Ru atoms. The unit cell of the stoichiometric $RuO_2(110)$ surface was found to consist coordinatively

unsaturated ruthenium atom (Ru_{cus}) which was not capped by any oxygen. The higher reactivity of oxide surface was explained by the formation of a kind of dangling bond via Ru_{cus} atom. When the oxygen coverage increased, due to weaker bonding of oxygen atoms on ruthenium oxide surface, CO reacts instead of desorption. This phenomena also emphasized the higher reactivity of oxide surface for CO oxidation [47].

Further research conducted about the formation of oxygen species on RuO_2 (110) surface, points out that very small activation barriers are measured during dissociative adsorption of oxygen across adjacent vacant site. It was identified that molecular O_2 structures are metastable on both cus and bridge surface sites. They easily dissociate for formation of atomic oxygen on vacant bridge or coordinatively unsaturated site (cus) of the surface [48].

All these studies about structure and reactivity provides insight for the modeling of both stoichiometric RuO_2(110) and RuO_2-O_Y surfaces. Calculated bulk lattice constants are found as a = 4.55 and b = 3.14 Å for the construction of supercell model of rutile structure with P42/mnm space group and space number of 136. Lattice parameter calculation is conducted with (15x15x15) k-points with 500 eV energy cut-off value. Periodic surface supercell with 2x1 is separated with the vacuum distance of 15 Å to diminish the unphysical interactions between the images in z-direction. Throughout the calculations, one layer of oxygen and one layer of ruthenium atoms present at the bottom layer of the surface have been kept fixed in all directions. Remaining of the surface is kept relaxed in all directions.

Optimized surface model used throughout the calculations for RuO_2(110) surface is shown as top view and side view respectively in Figure 3.2 (a) and (b).

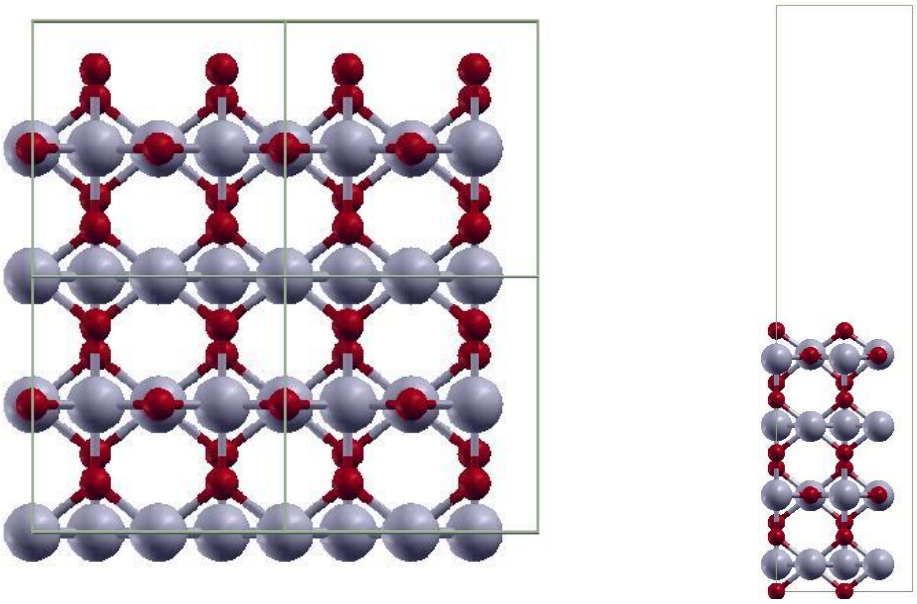

(a) Top view (b) Side view

Figure 3.2: Optimized $RuO_2(110)$ surface where smaller red atoms represent oxygen atoms and larger blue atoms represent ruthenium atoms

Literature survey revealed the coverage of non-lattice oxygen atoms, identified as O_γ species, on top of Ru_{cus} species in the presence of oxygen molecules in reaction medium. Since propylene epoxidation reaction takes place in an oxygen rich environment, RuO_2-O_γ surface has also been modeled and optimized as shown from top and side views in Figure 3.3 (a) and (b).

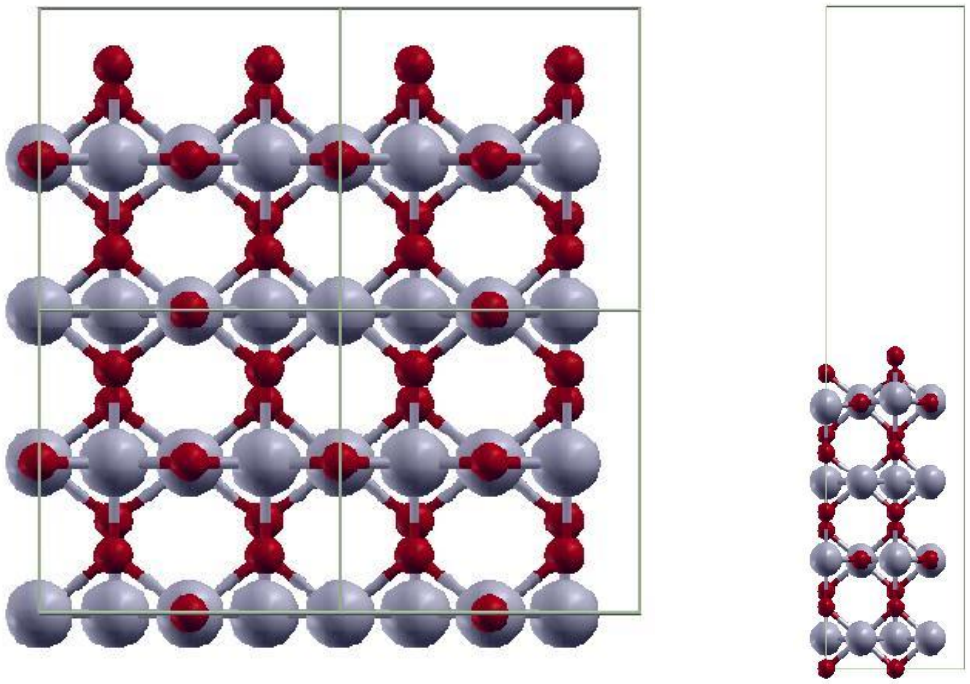

(a) Top view (b) Side view

Figure 3.3: Optimized RuO_2-O_γ surface where smaller red atoms represent oxygen atoms and larger blue atoms represent ruthenium atoms

Throughout the study, both $RuO_2(110)$ and RuO_2-O_γ surfaces have been studied for all reactions steps of propylene epoxidation mechanism. Atomic species of the surfaces are mainly located on bridge and coordinatively unsaturated sites (cus), namely Ru_{br}, Ru_{cus}, O_{br} and O_γ. All these atomic species positioned on the surface are shown in Figure 3.4. RuO_2 (110) surface includes Ru_{br}, Ru_{cus}, O_{br}; whereas RuO_2-O_γ surface includes Ru_{br}, Ru_{cus}, O_{br} and O_γ. Reactive oxygen that propylene activates for PO or side product formation is O_{br} for the $RuO_2(110)$ surface. Similarly for RuO_2-O_γ surface, reactivity of O_γ species has been taken into consideration for propylene epoxidation reactions steps.

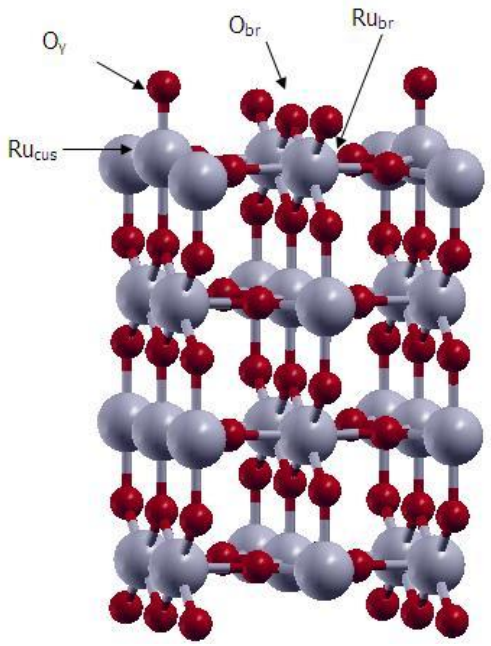

Figure 3.4: Ru_{br}, Ru_{cus}, O_{br} and O_γ species on $RuO_2(110)$ surface

3.4. Energy Profile Calculations

After optimization of catalytic slabs, $Cu_2O(001)$, $RuO_2(110)$ and RuO_2-O_γ surfaces, all reactants are products are modeled on the surfaces. Energies of optimized models with product or reactant on the corresponding surface have been calculated. Relative energies of all steps throughout the mechanism of propylene epoxidation are evaluated. All the steps of the reaction mechanism are determined [49]. Investigated steps throughout the study are given below:

Step 1 Surface + Propylene (g) → Surface-Propylene (ads)

Step 2 Surface-Propylene (ads) → Surface-OMMP1

Step 3 Surface-Propylene (ads) → Surface-OMMP2

Step 4 Surface-Propylene (ads) → Surface-H-Allyl Radical (ads)

Step 5 Surface-H-Allyl Radical (ads) → Surface-H + Allyl Radical (g)

Step 6 Surface-OMMP1 → Surface - Propylene oxide (ads)

Step 7 Surface-OMMP2 →Surface - Propylene oxide (ads)

Step 8 Surface-Propylene oxide (ads) → Surface (-1 Oxygen) + Propylene oxide (g)

Step 9 Surface - OMMP1 → Surface - Propionaldehyde (ads)

Step 10 Surface - Propionaldehyde (ads) → Surface (-1 Oxygen) + Propionaldehyde (g)

Step 11 Surface-OMMP2 → Surface - Acetone (ads)

Step 12 Surface - Acetone (ads) → Surface (-1 Oxygen) + Acetone (g)

Step 13 Surface + Propylene (g) → Surface - Propylene oxide (ads)

Step 1 is the adsorption of propylene on the surface. Propylene adsorption is followed by OMMP1 or OMMP2 formations on the surface shown as steps 2 and 3 respectively. Step 4 indicates the competing reaction with OMMP formations. This step is the allylic hydrogen stripping (AHS). Step 5 represents desorption of allyl radical from the surface. Step 6 and step 7 both stands for formation of propylene oxide (PO) either from OMMP1 or OMMP2. Propylene desorption from the surface is designated in step 8. Step 9 and step 10 are for formation and desorption of propionaldehyde respectively. Acetone formation and desorption steps are demonstrated in step 11 and step 12. In the study, formation of propylene oxide directly from

propylene without formation of surface intermediate is also investigated. This pathway is examined as step 13 throughout the steps of the mechanism.

Specifically for Cu_2O (001) surface, formation of acrolein has also been analyzed with step number of Step 14 and Step 15 as follows. Step 14 indicates the stripping of second hydrogen and formation of acrolein which is adsorbed to the surface. Step 15 presents desorption of acrolein where the surface remains with double hydrogen molecules connected to it.

Step 14 Surface-H-Allyl Radical (ads) → Surface-H-H-Acrolein (ads)

Step 15 Surface-H-H-Acrolein (ads) → Surface-H-H + Acrolein (g)

Relative energies of all steps are calculated as the difference between the summation of the energies of the products and summation of the energies of the reactants.

$$E_{(\text{relative energy})} = E_{\Sigma(\text{energies of the products})} - E_{\Sigma(\text{energies of the reactants})} \quad (3.1)$$

Activation barriers are investigated by CI-NEB analysis which leads to the characterization of transition state structure between the initial state and the final state of each step.

$$E_{(\text{activation barrier})} = E_{(\text{energy of the transition state})} - E_{(\text{energy of the initial state})} \quad (3.2)$$

Reactants and products of all steps of the reaction mechanism together with corresponding surface intermediates are shown in Figure 3.5.

Allylic hydrogens, which are bound to carbon atom of propylene, are shown as C3 in Figure 3.5. They are prone to be stripped by the oxygen atoms that are present on the catalytic surfaces. Stripping of hydrogen totally blocks the formation of propylene oxide as the desired product and results in formation of highly reactive allyl radical. In most cases allylic hydrogen stripping is an

indicator of total combustion. However, another valuable product which is acrolein is highly possible by stripping of the second hydrogen which is again bound to C3 and replacement of stripped hydrogen with an oxygen atom.

Instead of stripping of hydrogen, propylene also forms surface intermediates as shown in Figure 3.5, namely oxametallacycle-1 (OMMP1) and oxametallacycle-2 (OMMP2) respectively. OMMP1 is the surface intermediate where C1 is connected to the surface oxygen atom and C2 is connected to metal atom of the surface. Therefore OMMP1 forms a cycle-like geometry on the catalytic surface. OMMP2 surface intermediate is the similar surface intermediate. However, in that case, the difference is that C2 is bound to oxygen and C1 is bound to metal atom of the surface.

OMMP1 surface intermediate results in propionaldehyde formation when the removal of the bond between the metal atom and C2 is followed by hydrogen transfer from C1 to C2. Likewise, cleavage of the bond between metal atom and C1 of OMMP2 surface intermediate together with transfer of hydrogen from C2 to C1 results in the formation of acetone. Alternatively, both surface intermediates results in propylene oxide formation which is the desired target product of this study. For both surface intermediates, propylene oxide formation begins with the removal of the bond between the metal atom of the catalytic surface and corresponding carbon atom. In the meantime, bond between C1-C2 and surface oxygen is formed in the form of a cycle without any transfer of hydrogen.

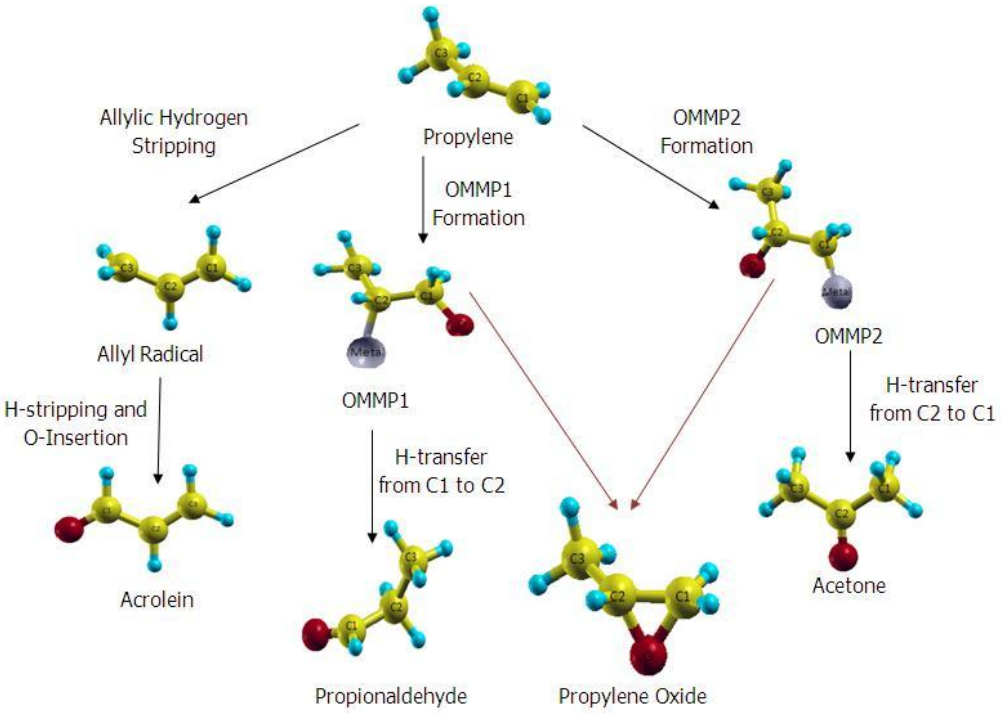

Figure 3.5: Propylene and the products that can be produced via propylene on catalytic surface

CHAPTER 4

RESULTS and DISCUSSION

This chapter presents the findings of the study. To remember, the purpose of this study is to understand the mechanism of propylene oxide formation on heterogeneous catalytic oxide surfaces, $Cu_2O(001)$ and $RuO_2(110)$. The steps of the mechanism are investigated together with the competing reactions which lead to products that block the formation of propylene oxide. DFT calculations have been conducted throughout the study for each of the steps in the mechanisms of the reactions.

4.1. Cu_2O (001) Surface

$Cu_2O(001)$ surface has been investigated for propylene epoxidation mechanism and all other competing mechanisms namely, stripping of hydrogen, formations of acetone and propionaldehyde.

Firstly, formations of surface intermediates, which are oxametallacycle 1 (OMMP1) and oxametallacycle 2 (OMMP2), have been analyzed in comparison with the competing mechanism which is stripping of hydrogen.

Analysis of formation of OMMP1 surface intermediate revealed that it is not possible to observe formation of OMMP1 on $Cu_2O(001)$ surface. The reason of this can be explained by the configuration of allylic group of the propylene molecule. When propylene is placed as OMMP1 structure on $Cu_2O(001)$

surface, hydrogen atoms of the allylic group remains very close to the oxygen atoms of the surface as seen in Figure 4.1. Distance between hydrogen and oxygen is found to be 1.77 Å. Hence, formation of the bond between oxygen and hydrogen is verified owing to such a close distance. Therefore, any possible configuration trials for OMMP1 structure resulted in stripping of allylic hydrogen by the surface oxygen.

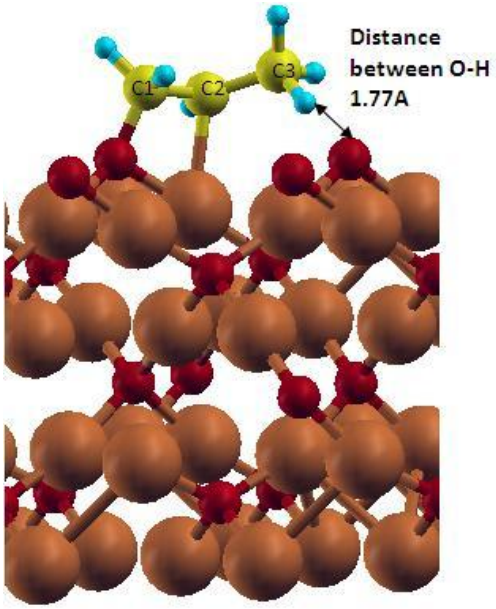

Figure 4.1: Configuration of OMMP1 structure on $Cu_2O(001)$ surface

OMMP2 formation and allylic hydrogen stripping (AHS) have been investigated in comparison with each other after the elimination of OMMP1 formation. Both OMMP2 formation and AHS have been presented to be exothermic reactions without activation barrier. Hence, transition state structures are not present. Initial and final state geometries of OMMP2 formations and stripping of allylic hydrogen are shown in Figure 4.2 and 4.3 respectively.

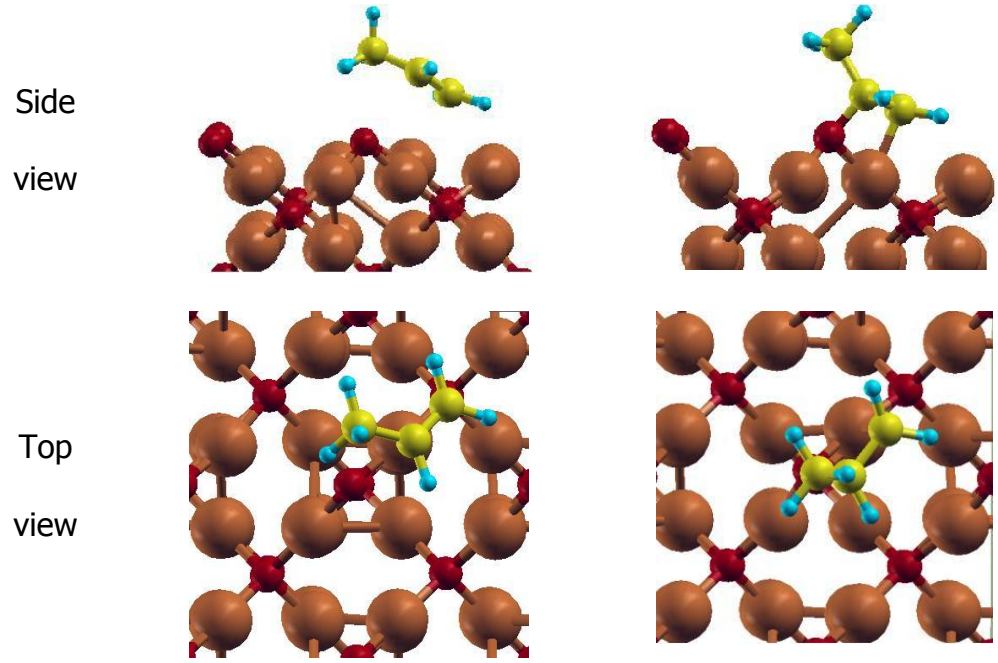

(a) Propylene Adsorption STEP 1 (b) OMMP2 formation STEP 3

Figure 4.2: Initial and final geometries of OMMP1 formation from propylene adsorption on $Cu_2O(001)$ surface

Formation of OMMP2 surface intermediate, as seen in Figure 4.2 (a), is presented starting from the adsorption of propylene, as seen in Figure 4.2 (b). Configuration of propylene is in a way that carbon atom, at the middle of propylene and named as (C2), approaches to surface oxygen whereas allyl group is positioned away from the surface oxygen. Propylene adsorption at the related configuration leads to OMMP2 formation without any activation barrier. Relative energy of this reaction is calculated to be -0.72 eV. Therefore, this step of the mechanism is an exothermic reaction without activation barrier.

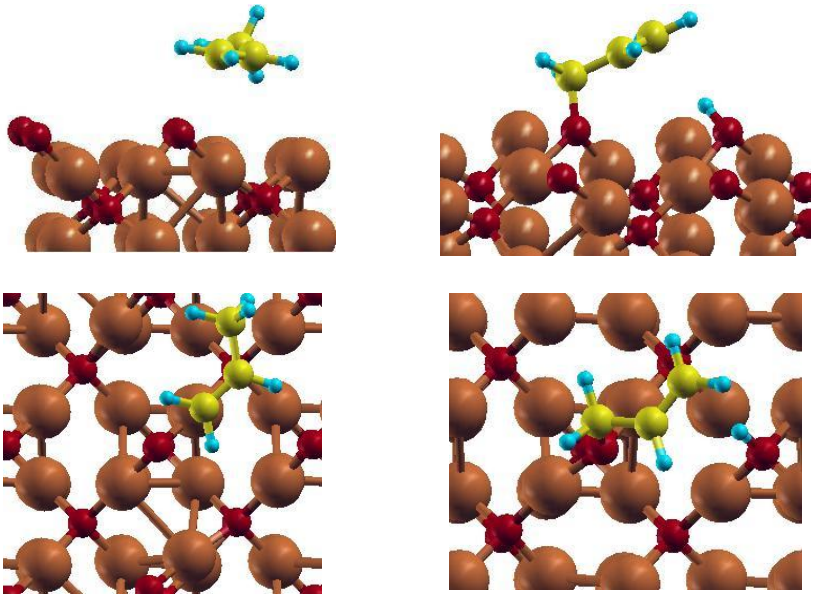

(a) Propylene Adsorption STEP 1 (b) AHS STEP 4

Figure 4.3: Initial and final geometries of allylic hydrogen stripping from propylene adsorption on $Cu_2O(001)$ surface

Figure 4.3 (a) presents the propylene configuration where propylene approaches to surface oxygen with the carbon atom, named as (C1) which is far away from the allylic group. Allylic group of propylene remains in a position where it is easily exposed to stripping. Hence, hydrogen of the allylic group is stripped to the surface oxygen as clearly seen in Figure 4.3 (b). Besides, allyl radical remains attached to the surface. Stripping of allylic hydrogen starting from the configuration of propylene adsorption in Figure 4.3 (a) has a relative energy of -2.28 eV and does not require a barrier.

Figure 4.4 shows the energy profile investigation of OMMP2 formation and AHS pathways. As stated, relative energy of OMMP2 formation is calculated to be -0.72 eV and relative energy of hydrogen stripping is found to be -2.28

eV which is much smaller than that of OMMP2 formation. Hence, AHS is more exothermic than OMMP2 formation. Steps that are after the formation of OMMP2 are not given in Figure 4.4 in order to avoid the complexity of the figure and they will be provided further in detail.

Figure 4.4 also presents desorption of allyl radical from the surface. The energy requirement for desorption of allyl radical is found to be 3.02 eV. Therefore it can be concluded that allyl is not going to desorp from the surface.

Considering the Cu_2O surface as a catalyst for acrolein formation, further reaction of allyl radical to acrolein formation has also been studied after the elimination of desorption of allyl radical from the surface owing to its high energy requirement of 3.02 eV. The pathway given in Figure 4.4 for acrolein formation shows the activation barrier for observing acrolein is 0.92 eV. Desorption of acrolein, which is indicated as formation of Step 15, has an energy requirement of 0.73 eV.

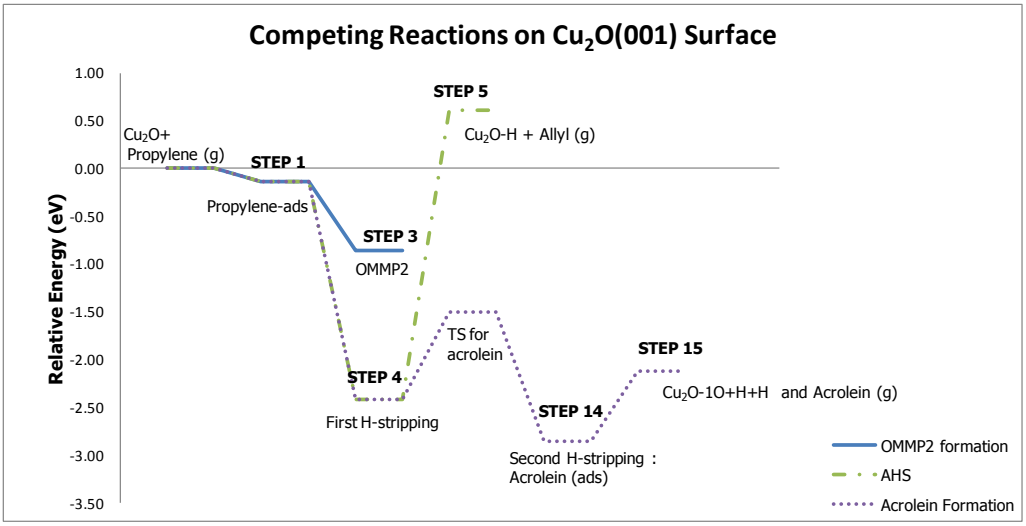

Figure 4.4: OMMP2 formation and AHS pathways on $Cu_2O(001)$ surface

Figure 4.5 shows initial, transition state and final states of acrolein formation. Acrolein formation initiates with stripping of first hydrogen as indicated in Figure 4.5 (a). So the geometry of AHS accounts for the initial state of acrolein formation. Then a transition state is shown in Figure 4.5 (b). At this geometry, hydrogen atom that is connected to carbon atom which has a bond with the surface oxygen starts to approach to the adjacent surface oxygen. The movement of the corresponding hydrogen stops when it makes the bond with surface oxygen. Ultimately acrolein formation as the final state is observed as noticed in Figure 4.5 (c). At this geometry, two of the surface oxygens are covered with hydrogen atoms.

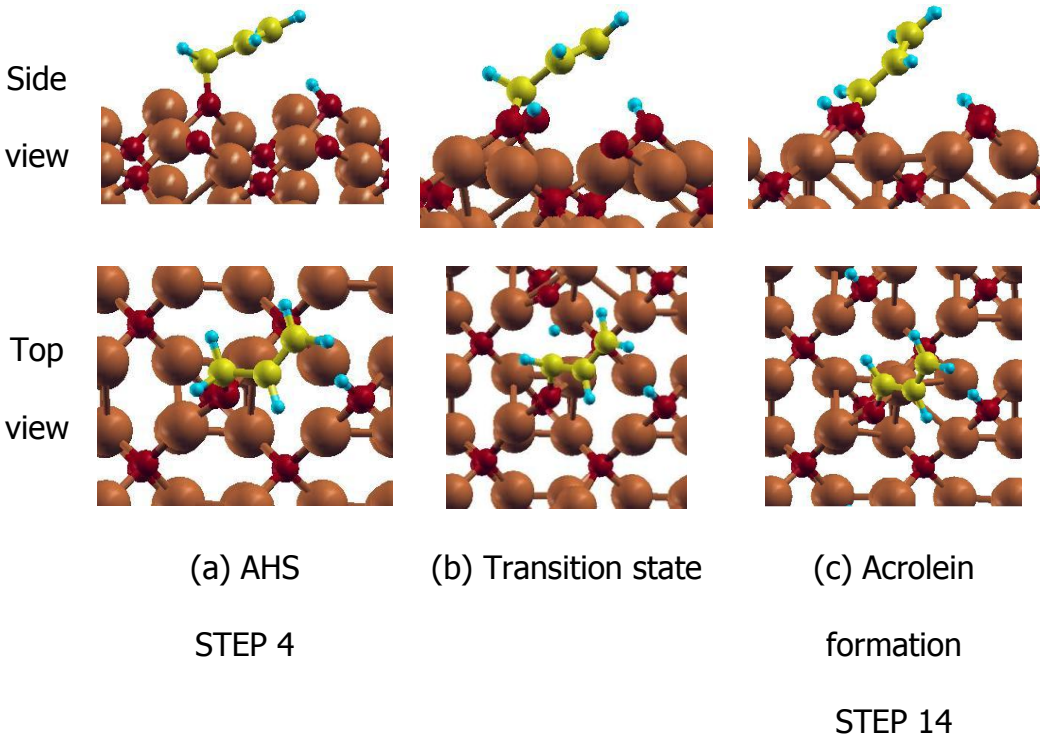

Figure 4.5: Initial, transition state and final geometries of acrolein formation from AHS on $Cu_2O(001)$ surface

OMMP2 surface intermediate is designated as Step3 in Figure 4.4 and it further goes on reaction to form PO or acetone. Figure 4.6 and 4.7 presents the formations of PO and acetone starting from initial geometries, followed by transition state geometries and ended by the final geometries respectively for each.

OMMP2 formation as seen in Figure 4.6 (a) is followed by the transition state where opening of the oxametallacyle ring is observed. C1 of the oxametallcacyle is disconnected from the copper atom of the Cu_2O (001) surface at transition state and it gets connected with the oxygen atom of the catalytic surface. Relative energy for PO formation from OMMP2 surface

intermediate is calculated to be 0.62 eV. Activation barrier analysis revealed the energy requirement of PO formation as 0.77 eV.

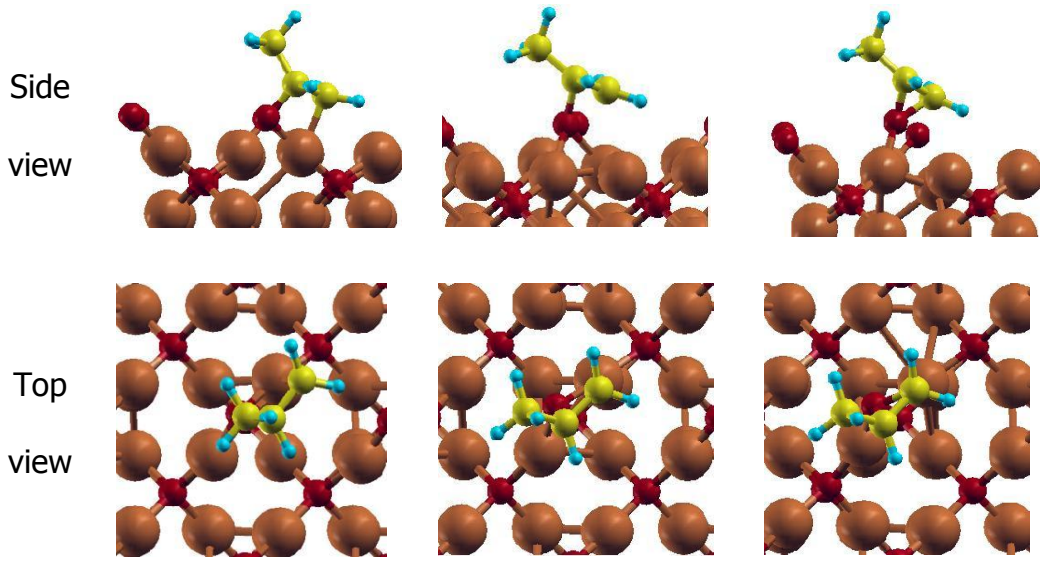

(a) OMMP2 (b) Transition state (c) PO

STEP 3 STEP 6

Figure 4.6: Initial, transition state and final geometries of PO formation from OMMP2 on $Cu_2O(001)$ surface

Acetone formation initiates by the formation of OMMP2 surface intermediate as seen in Figure 4.7 (a) and is an undesired step in the propylene oxide formation mechanism. In addition to ring opening of oxametallacyle surface intermediate, hydrogen atom that is connected to C2 starts to move to C1 of the structure as seen in the transition state at Figure 4.7 (b). The transfer of hydrogen from C2 to C1 leads to formation of acetone as seen in Figure 4.7 (c). Relative energy of this reaction is -1.26 eV and activation barrier is found as 0.59 eV.

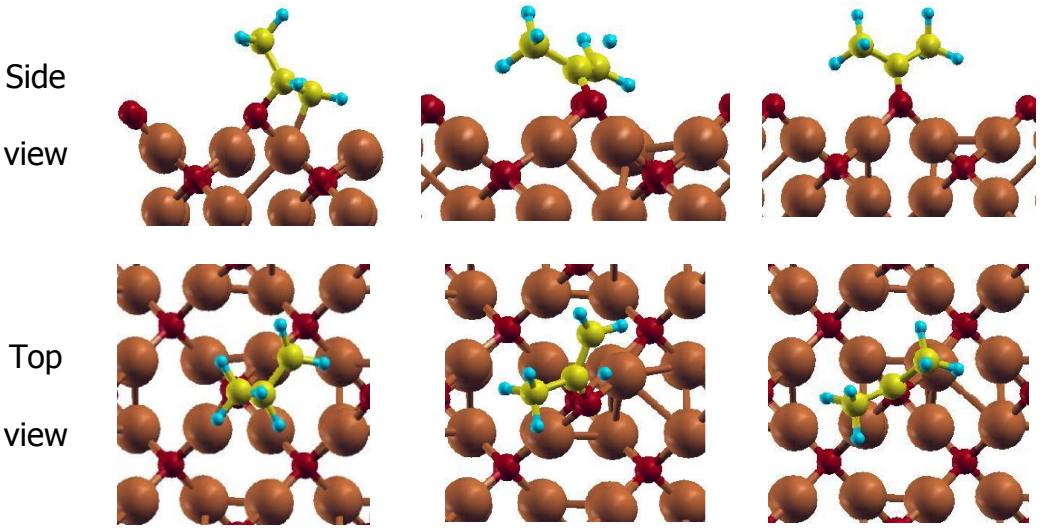

(a) OMMP2 (b) Transition state (c) Acetone

STEP 3 STEP 11

Figure 4.7: Initial, transition state and final geometries of acetone formation from OMMP2 on $Cu_2O(001)$ surface

Relative energy profile of PO and acetone formations on Cu_2O (001) surface is given in Figure 4.8. Activation barrier of acetone formation is found to be 0.59 eV. PO formation has a similar activation barrier and it has been found to be 0.77 eV. Desorption of acetone is 1.55 eV and desorption of PO is 0.84 eV energy requirement.

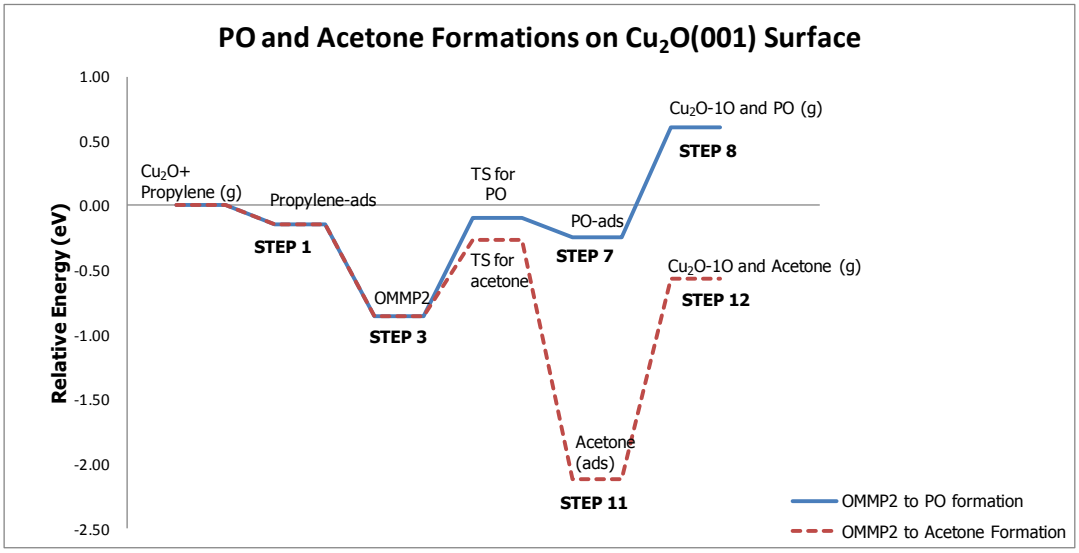

Figure 4.8: PO and acetone formations on $Cu_2O(001)$ surface through oxametallacycle pathway

Formation of PO directly without formation of the surface intermediate, OMMP, has also been a subject for the analysis. However, the calculations revealed that when propylene molecule approaches to the surface further than the distance of adsorption, it gets into interaction with the surface to form either OMMP2 surface intermediate or to strip one of the allylic hydrogen atoms. Propylene does not directly remove the oxygen atom of the Cu_2O (001) surface to form propylene oxide in any of the cases for direct mechanism.

4.2. RuO_2 (110) Surface

Propylene epoxidation mechanism together with side products and competing reactions have been analyzed firstly on RuO_2 (110) surface which is in fact stoichiometric RuO_2 (110) surface. Secondly O_Y species have been

modeled on RuO_2 (110) surface which provides RuO_2-O_γ (110) surface to study each mechanism steps.

4.2.1. RuO_2(110) Surface

Propylene oxide, acetone and propionaldehyde formations have been investigated through both oxametallacycle 1 (OMMP1) and oxametallacycle 2 (OMMP2) pathways on RuO_2(110) surface together with allylic hydrogen stripping to bridge oxygen (O_{br}) atom of the stoichiometric surface. Formation of propylene oxide by using O_{br} directly without any surface intermediate has also been a subject for analysis on RuO_2(110) surface.

Allylic hydrogen stripping (AHS) competes with OMMP1 and OMMP2 formations. Three of the reactions initiates with propylene adsorption on the surface. Initial, transition state and final geometries of OMMP1, OMMP2 and AHS formations are shown in Figure 4.9, 4.10 and 4.11 respectively.

Figure 4.9 (a) represents for the propylene adsorption geometry on RuO_2(110) surface. Propylene approaches to the empty site of the surface between two O_{br} atoms. C1 of the propylene gets into interaction with O_{br} atom and C2 makes a bond with the Ru_{cus} atom on the surface to form OMMP1 surface intermediate as seen in Figure 4.9 (c). Approximate transition state for formation of OMMP1 from propylene adsorption is given in Figure 4.9 (b). Relative energy of the reaction for formation of OMMP1 starting from propylene adsorption is -0.40 eV and activation barrier that propylene adsorption step needs to go beyond is 0.62 eV.

.

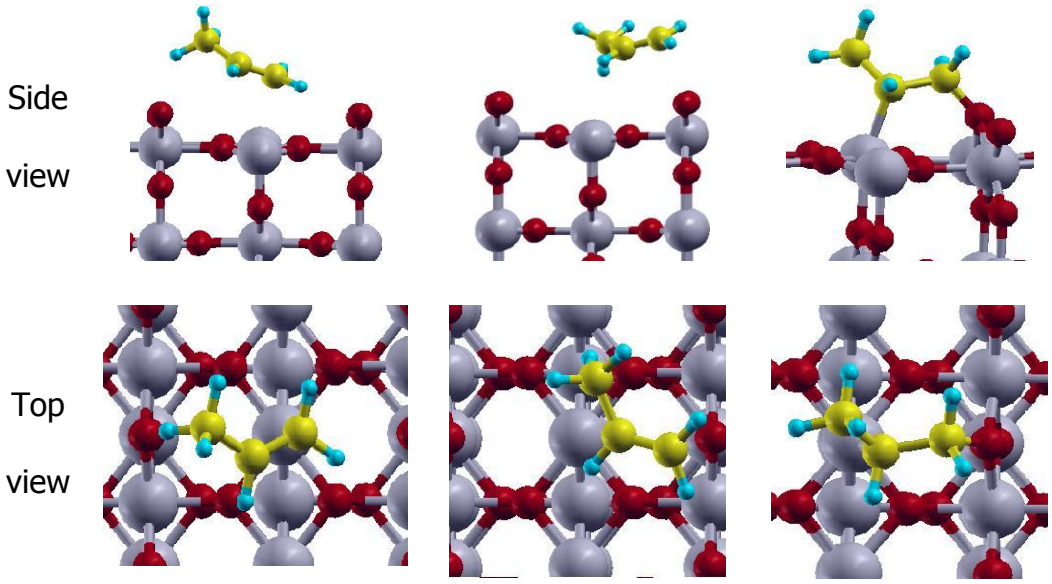

(a) Propylene Adsorption STEP 1 | (b) Approximate transition state | (c) OMMP1 formation STEP 2

Figure 4.9: Initial, approximate transition state and final geometries of OMMP1 formation from propylene adsorption on $RuO_2(110)$ surface

In Figure 4.10 (a), propylene adsorption is seen similar to Figure 4.9 (a). However, in this case C2 approaches to O_{br} and C1 makes a bond with Ru_{cus} on the surface as seen in Figure 4.10 (b). This interaction provides formation of OMMP2 surface intermediate as seen in Figure 4.10 (c). Relative energy of OMMP2 formation is calculated to be -0.53 eV with an activation barrier of 0.19 eV

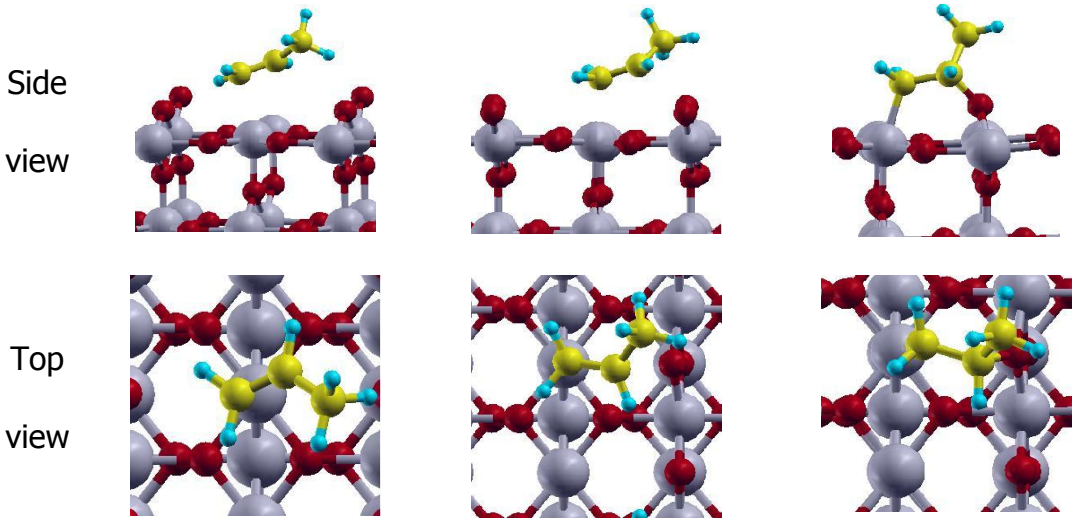

(a) Propylene Adsorption STEP 1 (b) Transition state (c) OMMP2 formation STEP 3

Figure 4.10: Initial, transition state and final geometries of OMMP2 formation from propylene adsorption on $RuO_2(110)$ surface

Propylene adsorption shown in Figure 4.11 (a) which is at the same site with Figure 4.9 (a) and 4.10 (a) has the tendency to result in allylic hydrogen stripping. As seen in Figure 4.11 (b), hydrogen atom of the allylic group is transferred to the bridge oxygen where 0.34 eV barrier of activation is needed. Finally, hydrogen is connected with O_{br} and remaining allyl radical makes a bond with Ru_{cus} as seen in Figure 4.11 (c). Relative energy of formation of step 4 is found as -0.19 eV when propylene adsorption accounts for the initial step.

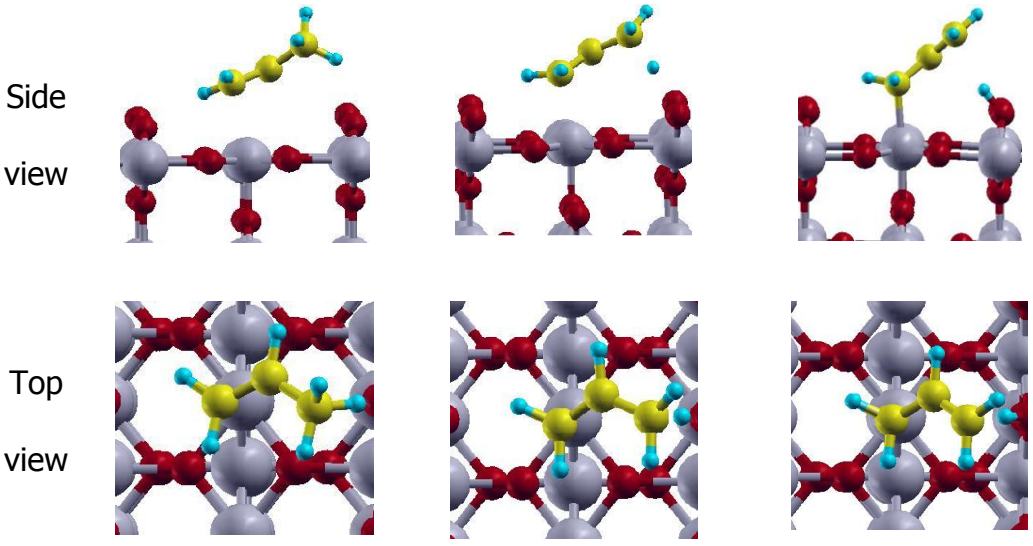

(a) Propylene Adsorption STEP 1 (b) Transition state (c) AHS STEP 4

Figure 4.11: Initial, transition state and final geometries of allylic hydrogen stripping (AHS)from propylene adsorption on RuO_2(110) surface

Activation barrier for OMMP1, OMMP2 formations and allylic hydrogen stripping are close to each other indicating that formations of these three steps are comparably possible to be observed as seen in Figure 4.4. After AHS, desorption of allyl radical has an energy requirement of 1.88 eV. So that further reaction steps could possibly be followed after AHS. These further steps, following AHS, would possibly lead to complete oxidation and certainly blocks formation of PO. OMMP1 and OMMP2 formations as indicated by Step 2 and Step 3 in Figure 4.4 further reacts and these reactions are also analyzed deeply; even they are not given in Figure 4.12.

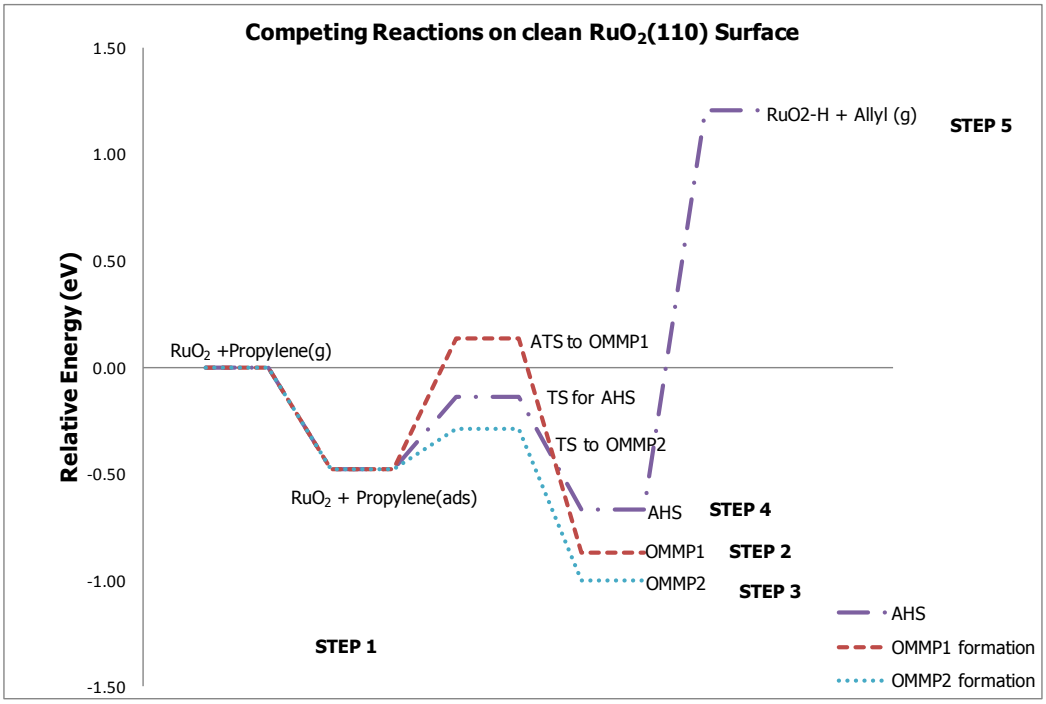

Figure 4.12: OMMP1, OMMP2 formations and AHS pathways on $RuO_2(110)$ surface

OMMP1 and OMMP2 surface intermediates are followed by PO formation, which is the desired product, or PA and acetone formations, which are side products. Formations of all of these are shown in Figure 4.13, 4.14, 4.15 and 4.16 where initial, transition state and final states are shown clearly from top and side views.

OMMP1 surface intermediate as shown in Figure 4.13 (a) leads to PO formation when the ring, which is formed by oxametallacycle, starts to open as seen in transition state structure shown in Figure 4.13 (b). Bond between C2 and Ru_{cus} is broken. This is followed by formation of the bond between C2 and Obr leading to formation of propylene oxide as seen in Figure 4.13 (c).

Relative energy between OMMP1 and PO formation is 1.33 eV with and activation barrier of 1.47 eV.

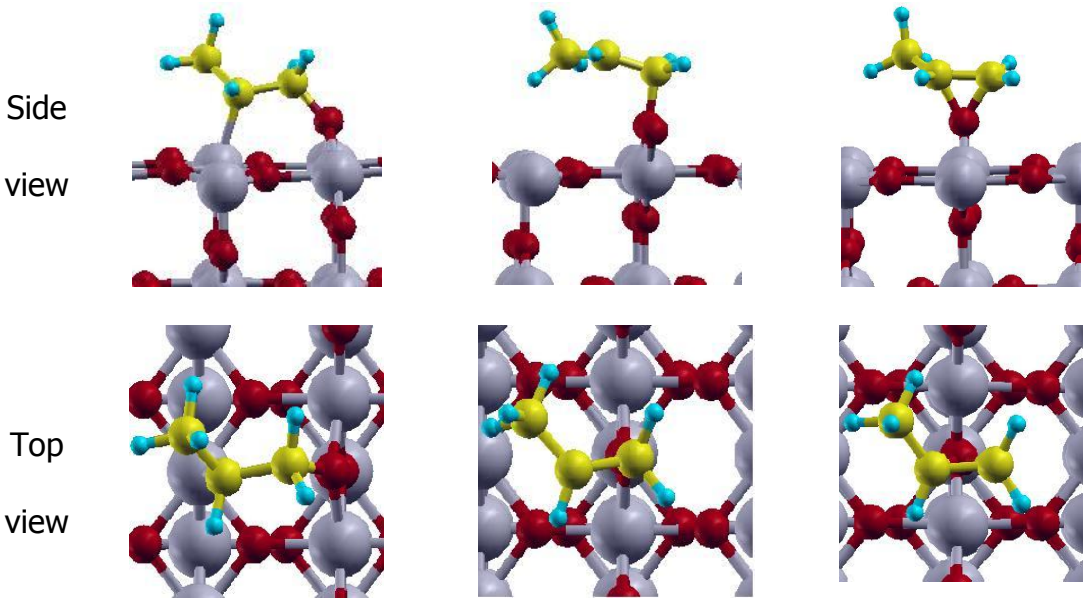

(a) OMMP1 (b) Transition state (c) PO

STEP 2 STEP 6

Figure 4.13: Initial, transition state and final geometries of PO formation from OMMP1 on RuO_2(110)surface

Figure 4.14 (a) represents the optimized OMMP2 surface intermediate placed on top of RuO_2 surface. OMMP2 surface intermediate forms with no activation barrier. However, since the reaction is an endothermic step, from OMMP2 to PO structure there's an energy requirement and the relative energy of PO formation through OMMP2 surface intermediate on RuO_2 surface is calculated to be 1.47 eV. Ultimately related pathway results in propylene oxide formation as the final product as seen in Figure 4.14 (c).

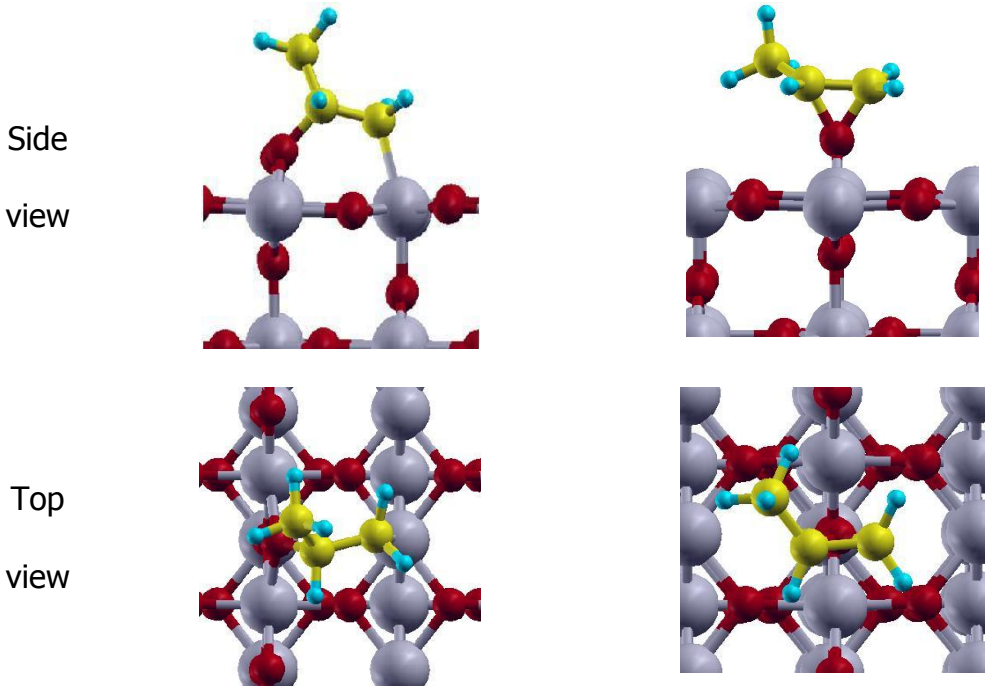

(a) OMMP2 (c) PO

STEP 3 STEP 6

Figure 4.14: Initial, transition state and final geometries of PO formation from OMMP2 on RuO_2(110)surface

Propionaldehyde (PA) forms from OMMP1 surface intermediate shown in Figure 4.15 (a), which is the same configuration also with Figure 4.13 (a). To achieve formation of PA, in addition to ring opening of the surface intermediate, hydrogen which has a bond with C1 is transferred to C2 as clearly seen in Figure 4.15 (b).Relative energy of the reaction to form PA geometry as seen in Figure 4.15 (c) is 0.48 eV. Activation barrier analysis revealed the energy requirement as 1.24 eV.

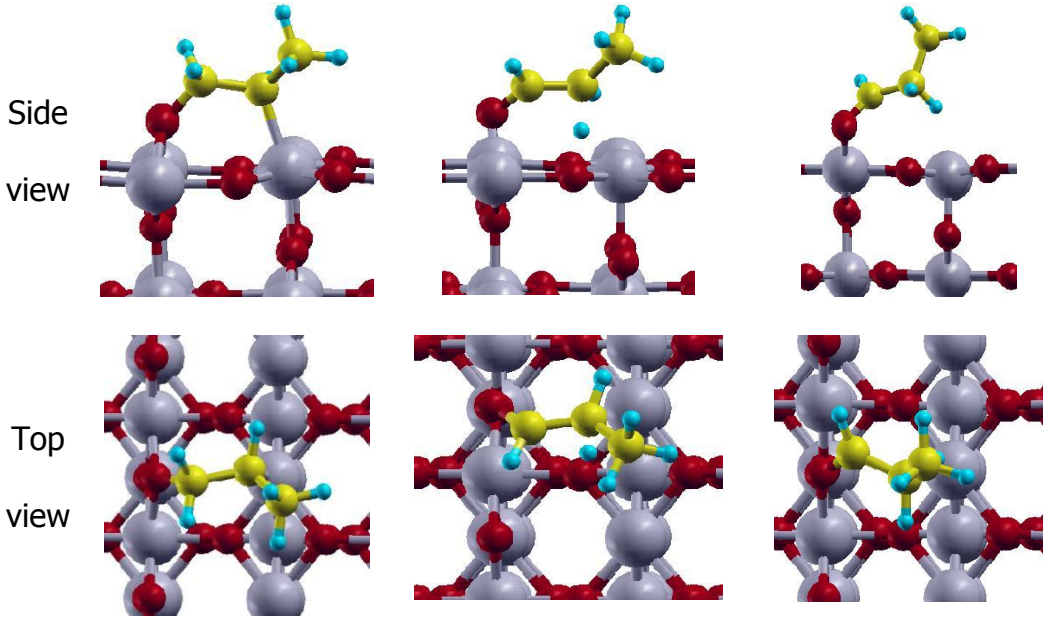

(a) OMMP1 (b) Transition state (c) PA

STEP 2 STEP 9

Figure 4.15: Initial, transition state and final geometries of PA formation from OMMP1 on RuO_2(110)surface

Figure 4.16 (a) represents the OMMP2 surface intermediate same as Figure 4.14 (a). Ring opening of the surface intermediate as seen in Figure 4.16 (b) together with transfer of hydrogen from C2 to C1 results in acetone formation as seen in Figure 4.16 (c). Relative energy of the corresponding reaction is calculated to be 0.05 eV. The activation barrier that is needed to be surpassed is 1.89 eV.

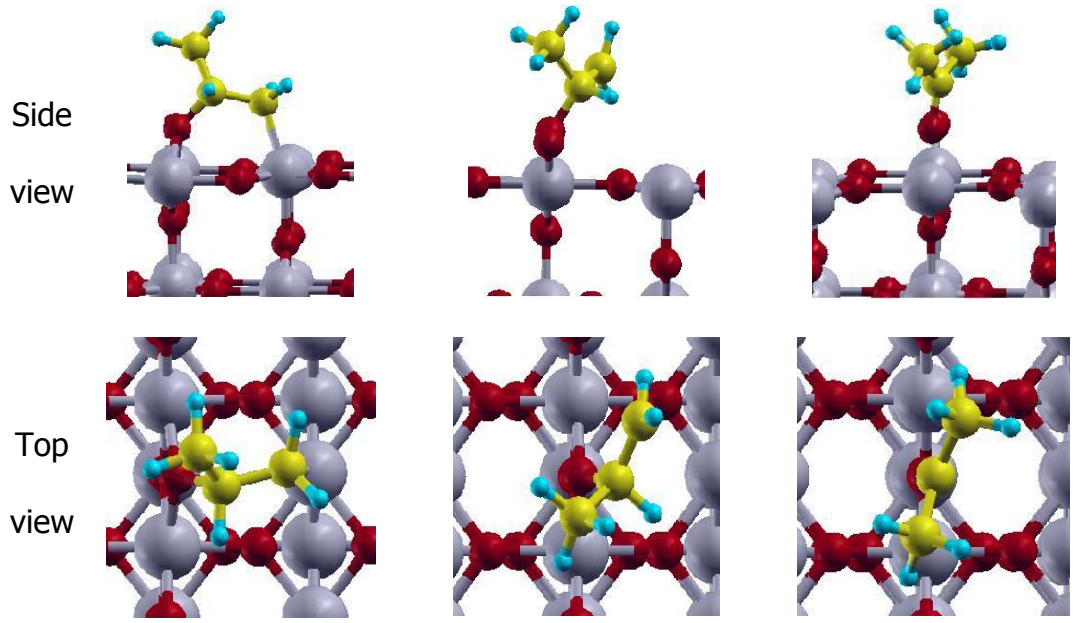

(a) OMMP1 (b) Transition state (c) Acetone

STEP 2 STEP 11

Figure 4.16: Initial, transition state and final geometries of acetone formation from OMMP2 on RuO_2 surface

PO formations through both surface intermediates, OMMP1 and OMMP2, have high activation barrier as seen in Figure 4.17. Acetone formation has the highest activation barrier. Activation barrier for PA formation has the lowest barrier when compared to others. Desorption energies of PO, PA and acetone are calculated to be 0.78, 0.81 and 1.03 eV respectively.

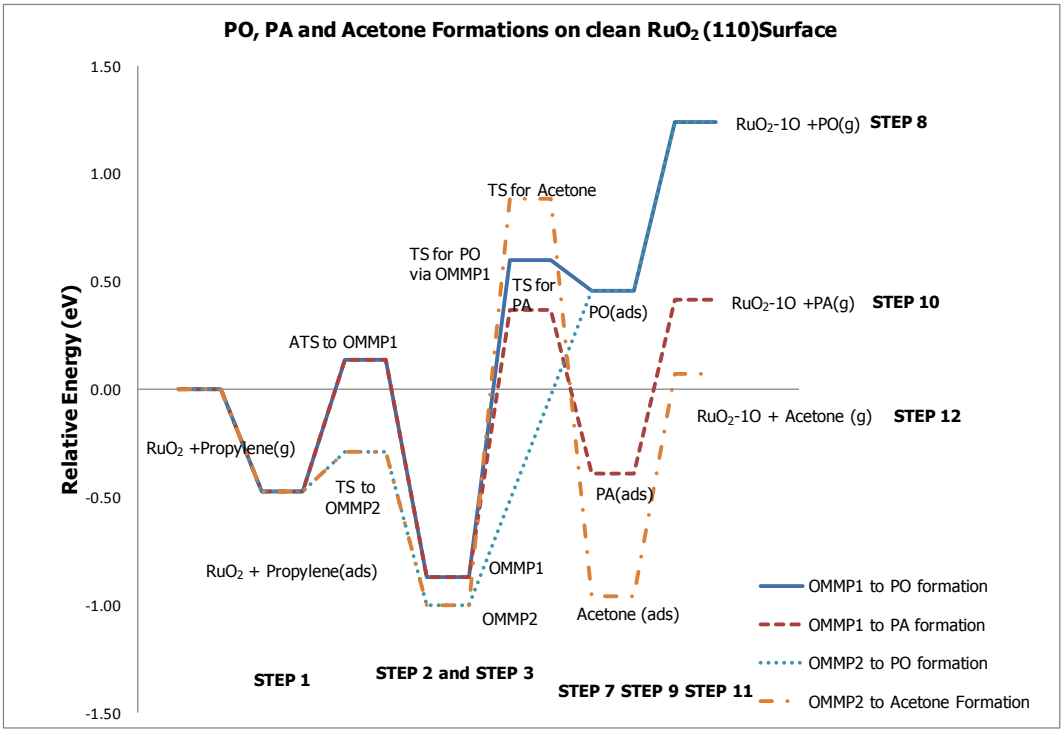

Figure 4.17: PO, PA and acetone formations on RuO_2(110) surface through oxametallacycle pathway

In addition to PO formation through oxametallacycle formation, direct PO formation, where propylene molecule removes O_{br}, has also been investigated. However in order to follow direct pathway, propylene molecule adsorbs on a different site. Site 1 is shown in Figure 4.18 for propylene adsorption geometry in chemisorbed state that may result in OMMP1, OMMP2 formations and allylic hydrogen stripping. Site 2 is physisorbed propylene adsorption geometry which is on top of O_{br} as shown in Figure 4.10. This geometry ends up in direct PO formation by insertion of O_{br} to propylene for PO formation.

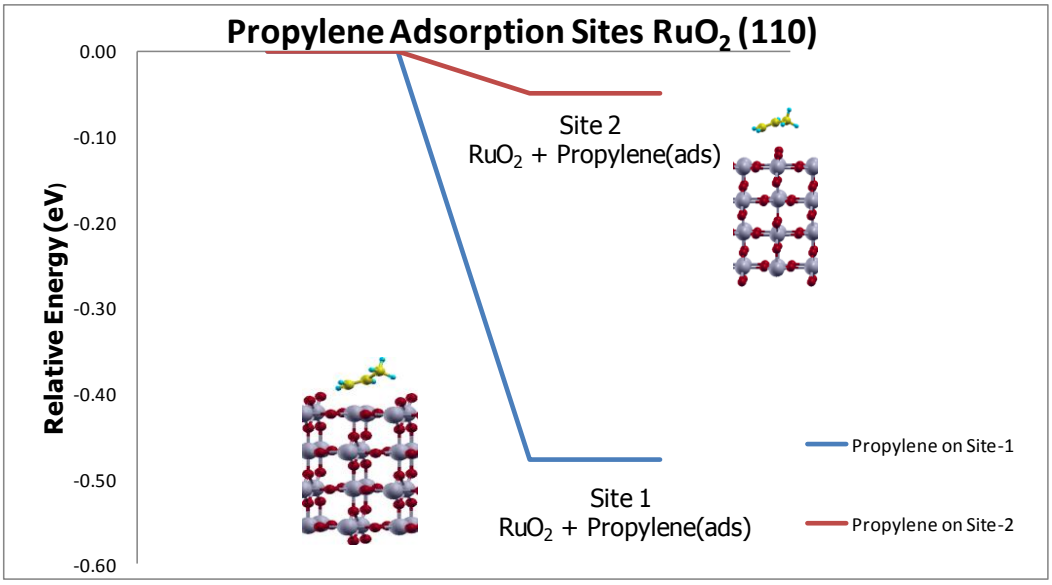

Figure 4.18: Propylene adsorption sites on $RuO_2(110)$ surface

During formation of PO, propylene follows the direct pathway instead of being adsorbed on site-1 for oxametallacycle formation. Initial, transition state and final geometries of direct propylene oxide formation is given in Figure 4.19.

Adsorption of propylene on top of O_{br} of the $RuO_2(110)$ surface is seen in Figure 4.19 (a). Initially C2 of the propylene connects with O_{br} as seen in the transition state configuration in Figure 4.19 (b). Ultimately C1 completes the ring cycle of carbon-oxygen-carbon to form propylene oxide (PO) as seen in Figure 4.19 (c). Relative energy of the direct formation without any surface intermediate is calculated to be 0.51 eV. Activation barrier to form PO directly by O_{br} of the surface is found to be 0.81.

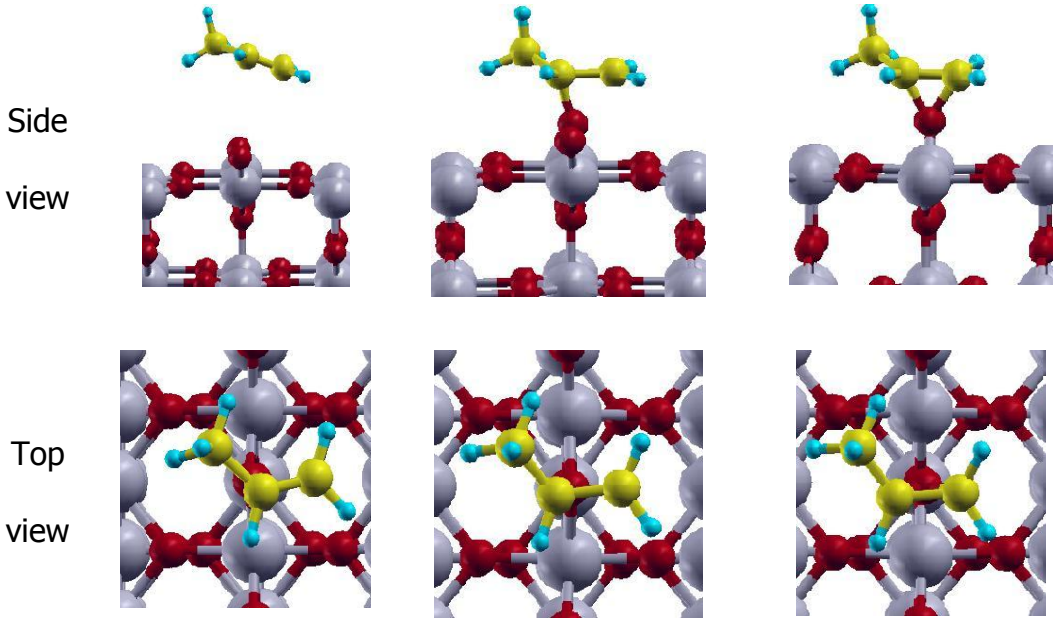

(a) OMMP1 (b) Transition state (c) PO

STEP 1 STEP 13

Figure 4.19: Initial, transition state and final geometries of PO formation directly from propylene physisorption on RuO_2(110) surface

It comes out that direct pathway has a less activation barrier of 0.81 eV as also seen in Figure 4.20. This result showed that oxametallacycle surface intermediate is a stable surface intermediate which makes PO formation almost impossible through oxametallacycle formation. Direct pathway is found as the most favorable mechanism which can enable PO formation via O_{br} on RuO_2 (110) surface.

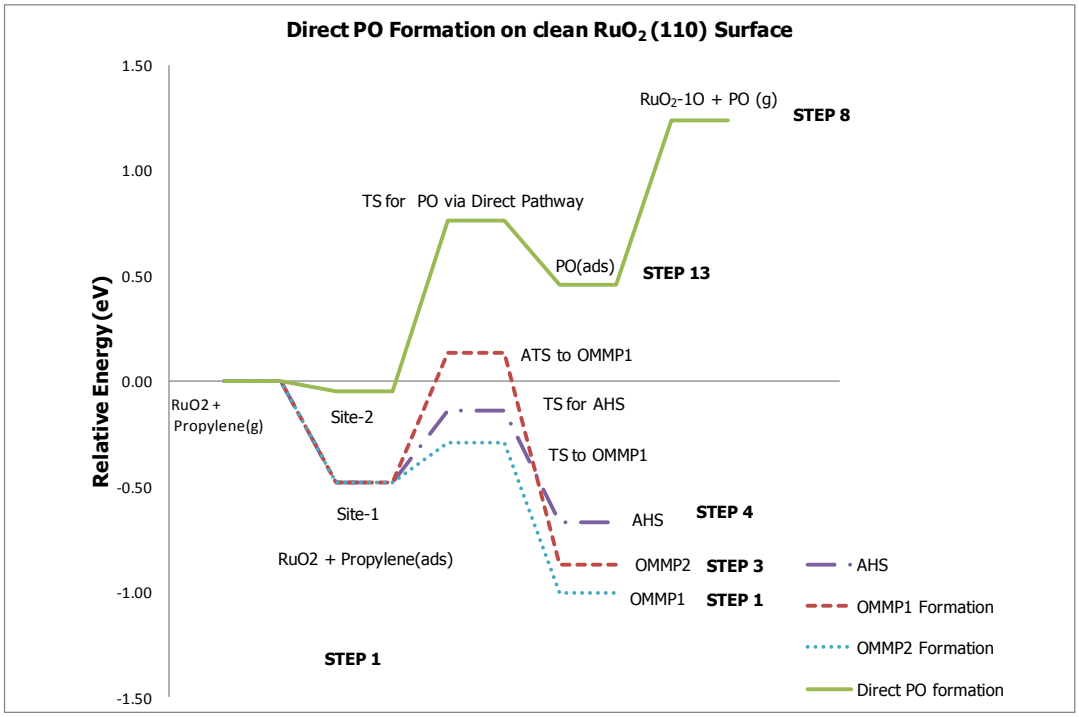

Figure 4.20: Direct PO formation and its competitive reactions on RuO_2(110) surface

4.2.2. RuO_2 (110) Surface with O_Y species

Instead of propylene adsorption on site 1, O_Y species are modeled on top of Ru-cus. So that propylene adsorption on this site is prevented due to the presence of O_Y species on this site. This surface is named as RuO_2-O_Y surface throughout the study. O_Y species are analyzed to see the activity of oxygen atoms that does not belong to lattice structure of the stoichiometric RuO_2 (110) surface.

Binding energies of O_{br} and O_Y species are compared in Table 4.1. O_{br} species are strongly bound to surface since they belong to stable lattice structure of RuO_2 (110) surface. O_Y species are relatively weakly bound oxygen species. This could possibly indicate higher activity for these species.

Since O_γ species are weakly bound, propylene could activate and remove them easier from the surface for formation of propylene oxide.

Table 4.1: Binding energies of oxygen species on RuO_2

Binding Energy (eV)	
O_{br} on RuO_2 (110)	-2.31
O_γ on RuO_2 (110)	-0.89

Competing reactions which are allylic hydrogen stripping (AHS), OMMP1 and OMMP2 formations have been analyzed on RuO_2-O_γ surface. Figure 4.21, 4.22 and 4.23 show initial, transition state and final state geometries of OMMP1, OMMP2 formations and AHS on RuO_2-Oγ surface.

Figure 4.21 (a) shows adsorption of propylene on RuO_2-O_γ surface on the site where it is surrounded by both two of O_γ species and two of the O_{br} species. C1 of propylene approaches to O_γ. After passing through the transition state geometry as seen in Figure 4.21 (b), with activation barrier of 0.30 eV. Formation of OMMP1 surface intermediate with relative energy of -0.54 eV where initial geometry is Figure 4.21 (a) and final geometry is 4.21 (c).

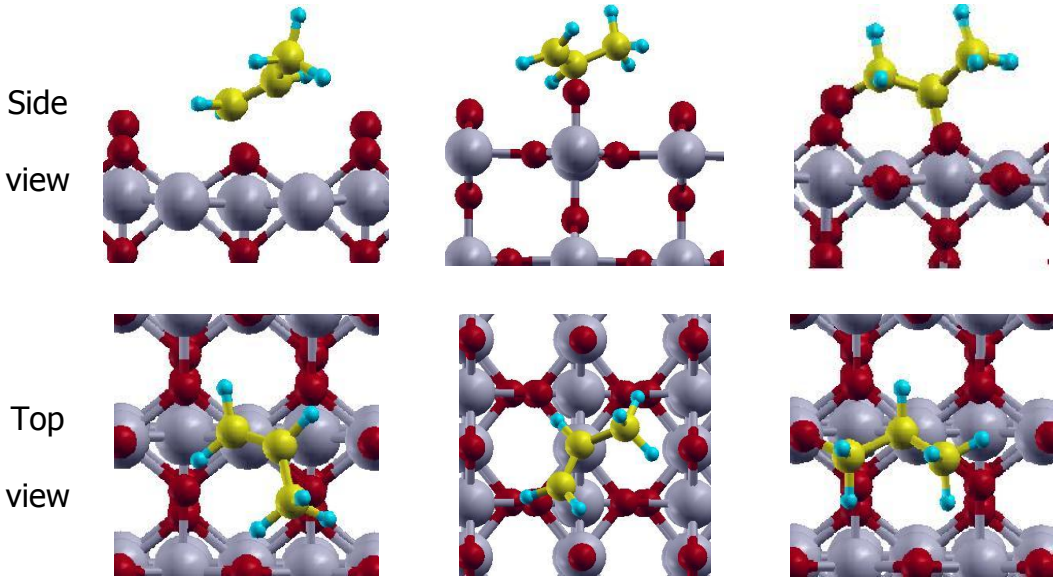

(a) Propylene adsorption STEP 1 (b) Transition state (c) OMMP1 STEP 2

Figure 4.21: Initial, transition state and final geometries of OMMP1 formation from propylene adsorption on RuO_2-O_γ surface

Propylene adsorption geometry in Figure 4.22 (a) is the same configuration with Figure 4.21 (a). In this case as seen in the transition state geometry for OMMP2 formation in Figure 4.22 (b), C2 of propylene approaches to adjacent O_γ species. Relative energy of the reaction for the formation of OMMP2 surface intermediate is found to be -0.77 eV. This reaction is almost an exothermic reaction without activation barrier since activation barrier analysis of the corresponding reaction has revealed the amount of barrier value as 0.05 eV.

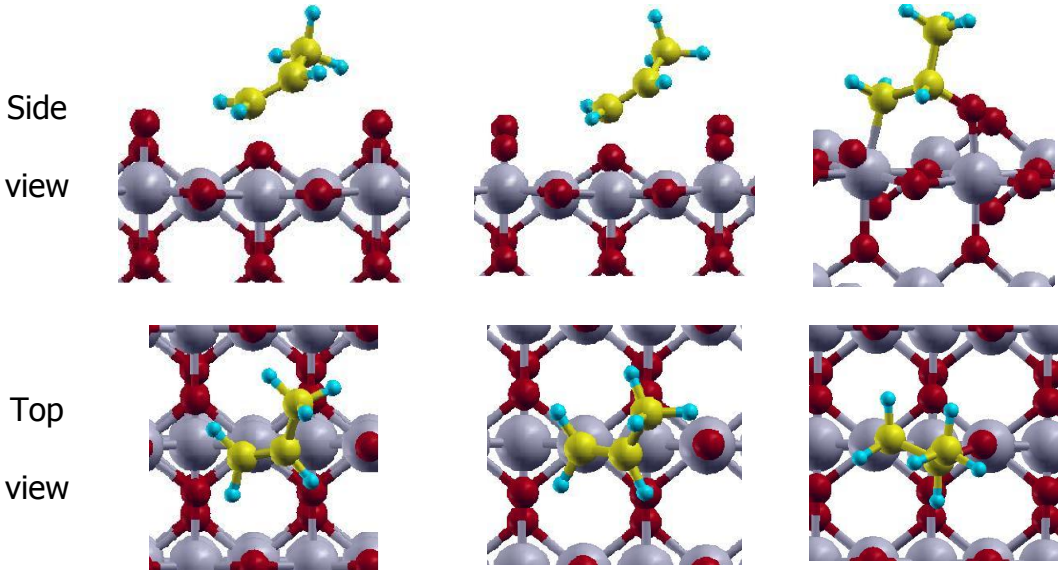

(a) Propylene adsorption STEP 1 (b) Transition state (c) OMMP2 STEP 3

Figure 4.22: Initial, transition state and final geometries of OMMP2 formation from propylene adsorption RuO_2-O_Y surface

Initiating from the similar propylene adsorption geometry which is surrounded by two different type of oxygen atoms (O_Y and Obr) at all the corners as seen in Figure 4.23 (a), stripping of allylic hydrogen to O_Y species is presented in Figure 4.23 (b). Transition state geometry of AHS given in Figure 4.23 (b) has activation energy requirement of 0.61 eV. Relative energy of allylic hydrogen stripping is 0.06 eV.

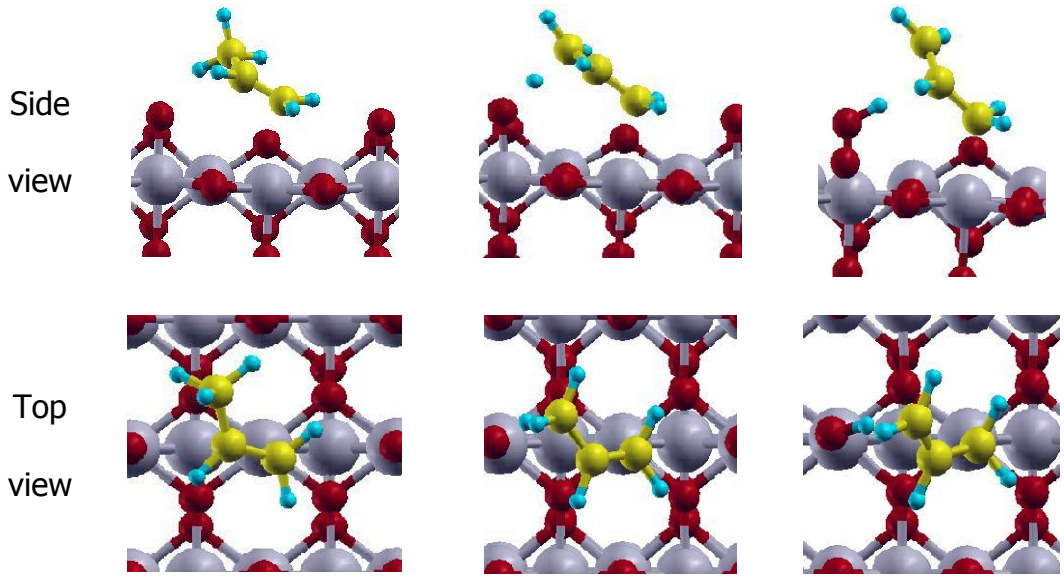

(a) Propylene adsorption STEP 1 (b) Transition state (c) AHS STEP 4

Figure 4.23: Initial, transition state and final geometries of AHS from propylene adsorption on RuO_2-O_Y surface

Transition state of AHS step requires 0.61 eV activation barrier value as seen in Figure 4.16. When AHS is compared with OMMP1 and OMMP2 formations, formation of OMMP2 surface intermediate is the most favorable pathway since it is an exothermic reaction almost without any activation barrier (0.05 eV). In other words, OMMP2 formation is most likely to be observed on RuO_2-O_Y surface.

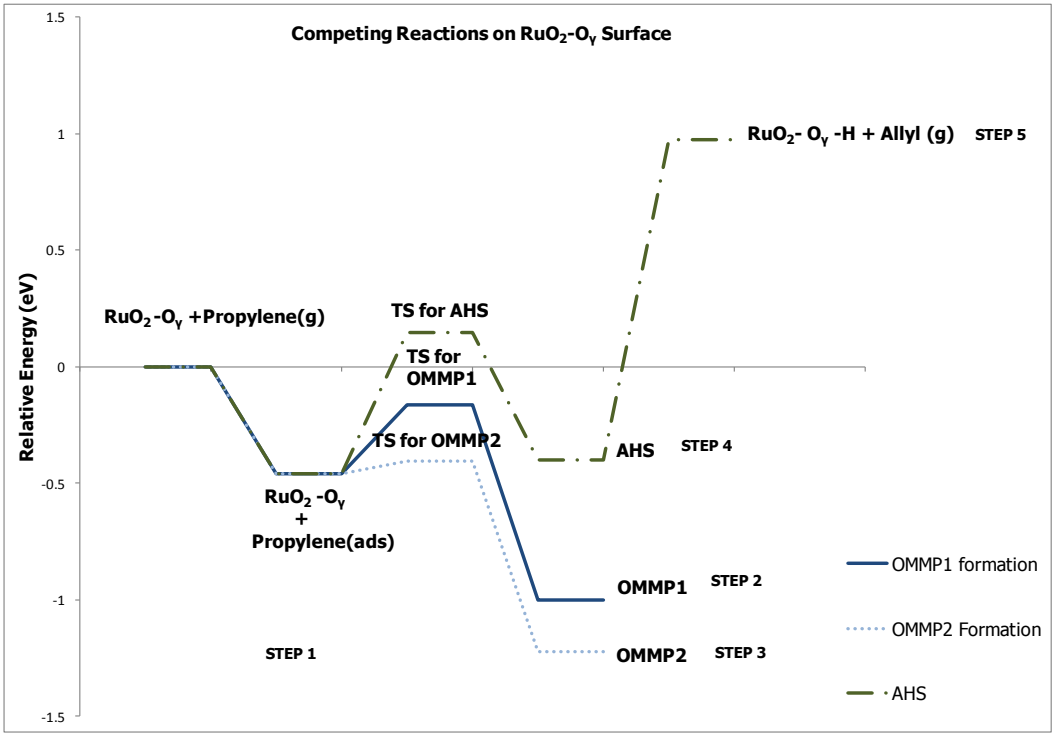

Figure 4.24: OMMP1, OMMP2 formations and AHS pathways on RuO_2-Oγ surface

After formations of OMMP1 and OMMP2 surface intermediates, PO, PA and acetone formations have been analyzed. Geometries of PO formations through OMMP1 and OMMP2 are shown in Figure 4.25 and 4.26 respectively. Figure 4.27 and 4.28 illustrates the geometries of PA and acetone formations through OMMP1 and OMMP2 surface intermediates respectively.

Figure 4.25 (b) indicates the surface intermediate, OMMP1 where the cycle is formed within O_Y species and Ru-cus which is in fact the same geometry with Figure 4.21 (c). Transition state geometry given in Figure 4.25 (b) is followed by formation of propylene oxide as seen in Figure 4.26 (c) with an activation energy requirement of 0.63 eV. Relative energy of the corresponding reaction on RuO_2-O_Y surface is calculated to be -0.26 eV.

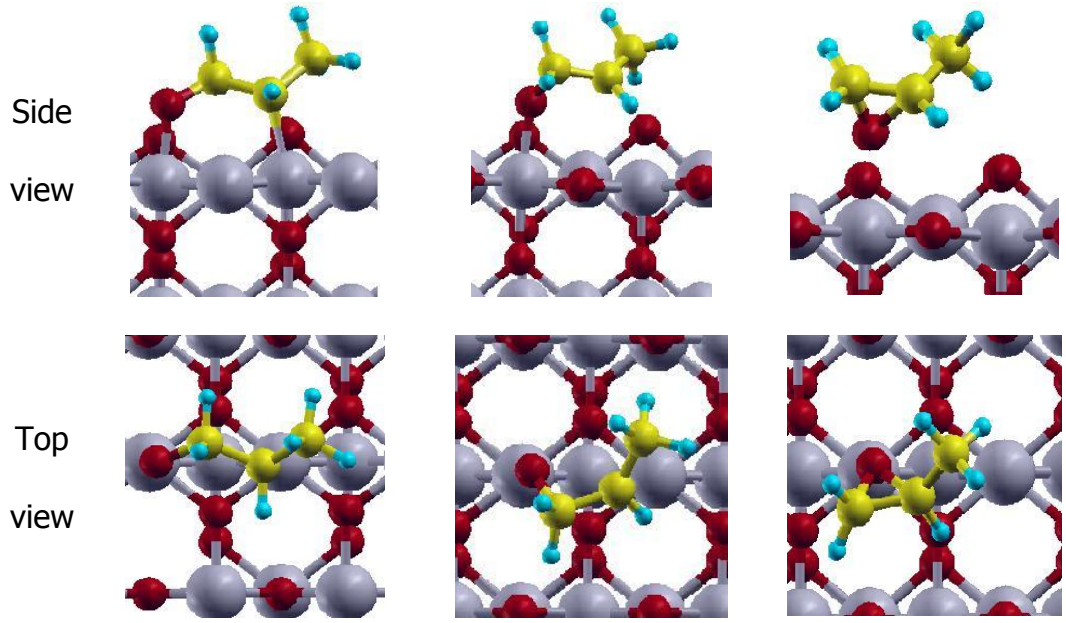

(a) OMMP1 (b) Transition state (c) PO

STEP 2 STEP 6

Figure 4.25: Initial, transition state and final geometries of PO formation from OMMP1 on RuO_2-O_γ surface

OMMP2 surface intermediate formed on RuO_2-O_γ surface is illustrated in Figure 4.26 (a) which is the same geometry as Figure 4.22 (c). The cycle of oxametallacycle ring is opened as seen in transition state geometry given in Figure 4.26 (b). Activation barrier of PO formation from OMMP2 surface intermediate is calculated to be 1.07 eV. Relative energy of the reaction is found to be -0.03 eV.

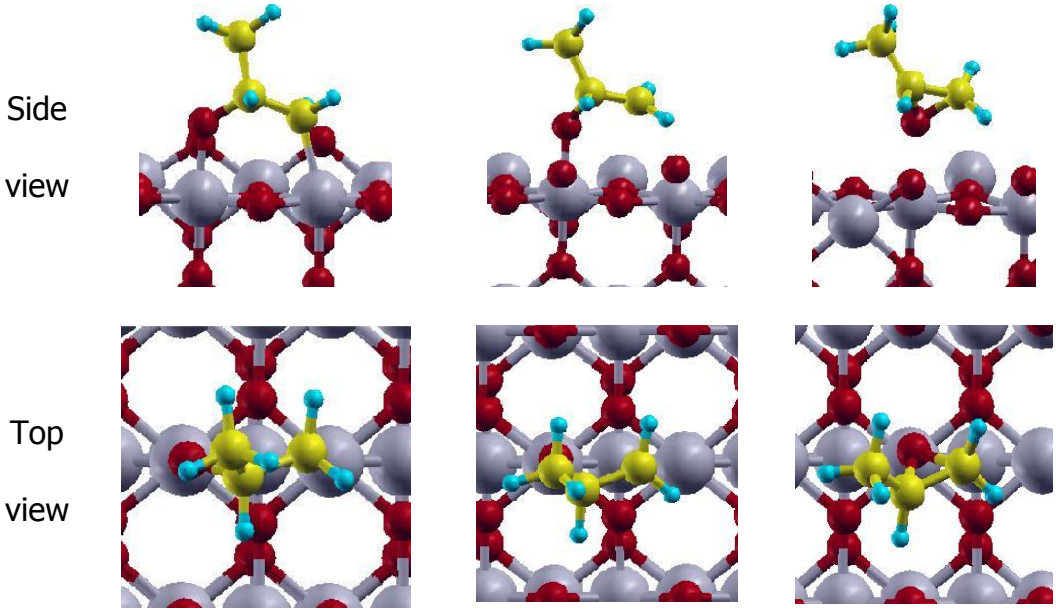

(a) OMMP2 (b) Transition state (c) PO

STEP 2 STEP 7

Figure 4.26: Initial, transition state and final geometries of PO formation from OMMP1 on RuO_2-O_γ surface

Figure 4.27 (a) is the OMMP2 surface intermediate which leads to PA formation as seen in Figure 4.27 (c) on RuO_2-O_γ surface. Relative energy of this reaction is calculated to be -1.00 eV. At the transition state geometry corresponding to PA formation hydrogen atom is transferred to C2 atom of the structure as seen in Figure 4.27 (b). Activation barrier analysis revealed the energy requirement of PA formation as 0.78 eV.

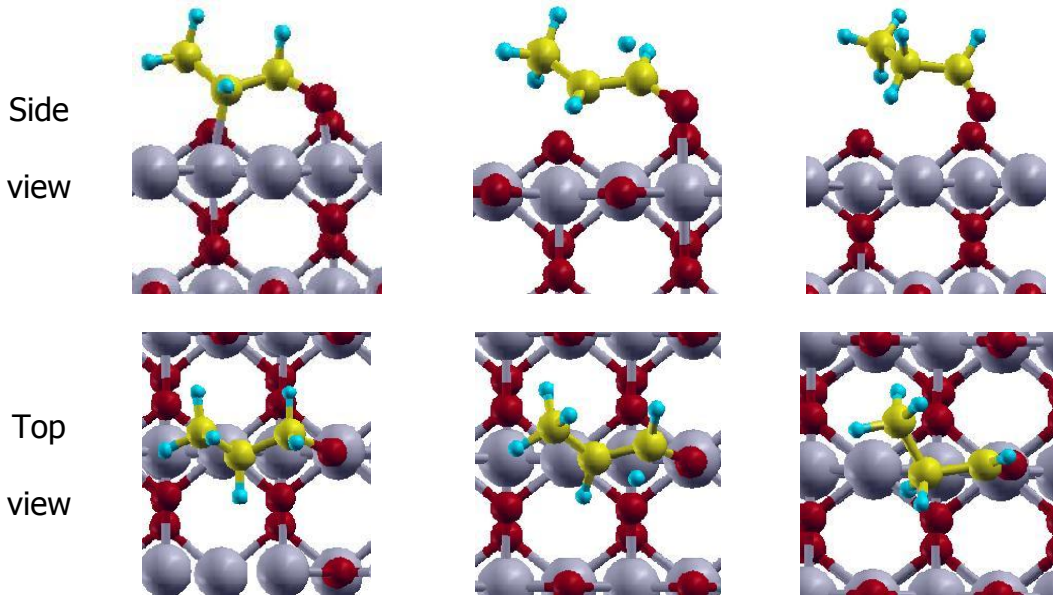

(a) OMMP2 (b) Transition state (c) PA

STEP 2 STEP 9

Figure 4.27: Initial, transition state and final geometries of PA formation from OMMP1 on RuO_2-O_Y surface

OMMP2 surface intermediate given in Figure 4.28(a) leads to acetone formation with the transfer of hydrogen from C2 to C1. Acetone formation is illustrated in Figure 4.28 (c) on RuO_2-O_Y surface. Relative energy of acetone formation starting from OMMP2 is found to be -1.16 eV. Transition state geometry of acetone formation is seen in Figure 4.28 (c). Activation barrier of acetone formation from OMMP2 surface intermediate is calculated to be 1.09 eV.

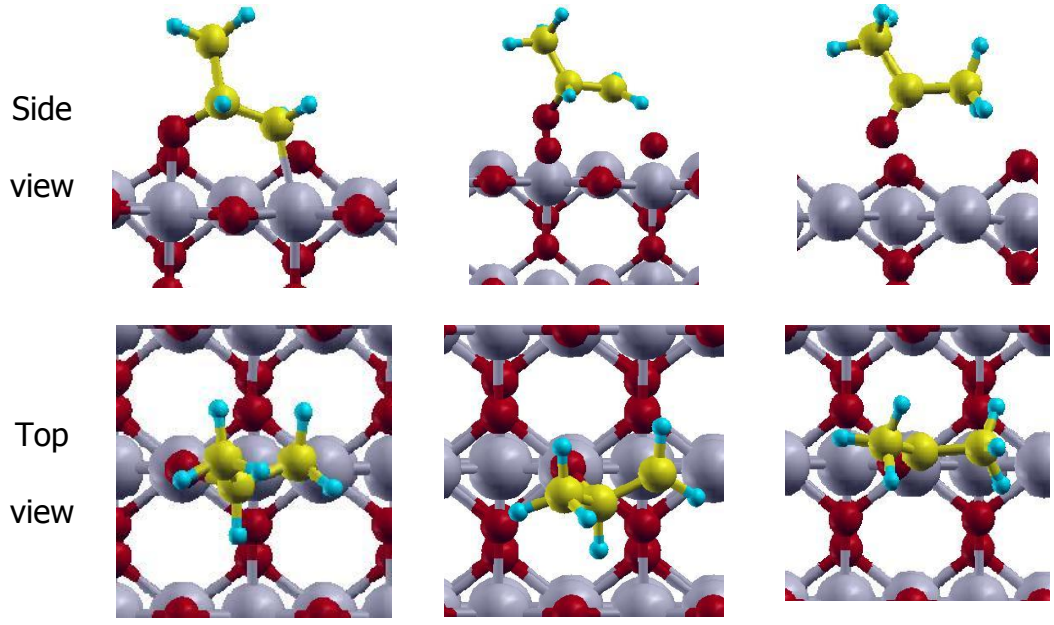

(a) OMMP2 (b) Transition state (c) Acetone

STEP 2 STEP 11

Figure 4.28: Initial, transition state and final geometries of acetone formation from OMMP2 on RuO_2-O_γ surface

The corresponding activation barrier values for PO, PA and acetone formations starting from corresponding surface intermediate, OMMP1 or OMMP2, are shown in Figure 4.21. OMMP1 formation has a higher activation barrier than OMMP2 formation. PA and PO formation upon formation of OMMP1 surface intermediate, both have similar activation barriers 0.78eV and 0.63 eV respectively. When most favorable surface intermediate, OMMP2, is taken into consideration, it can be obviously seen both PO and acetone formations are going to be favored similarly due to the same amount of activation barriers.

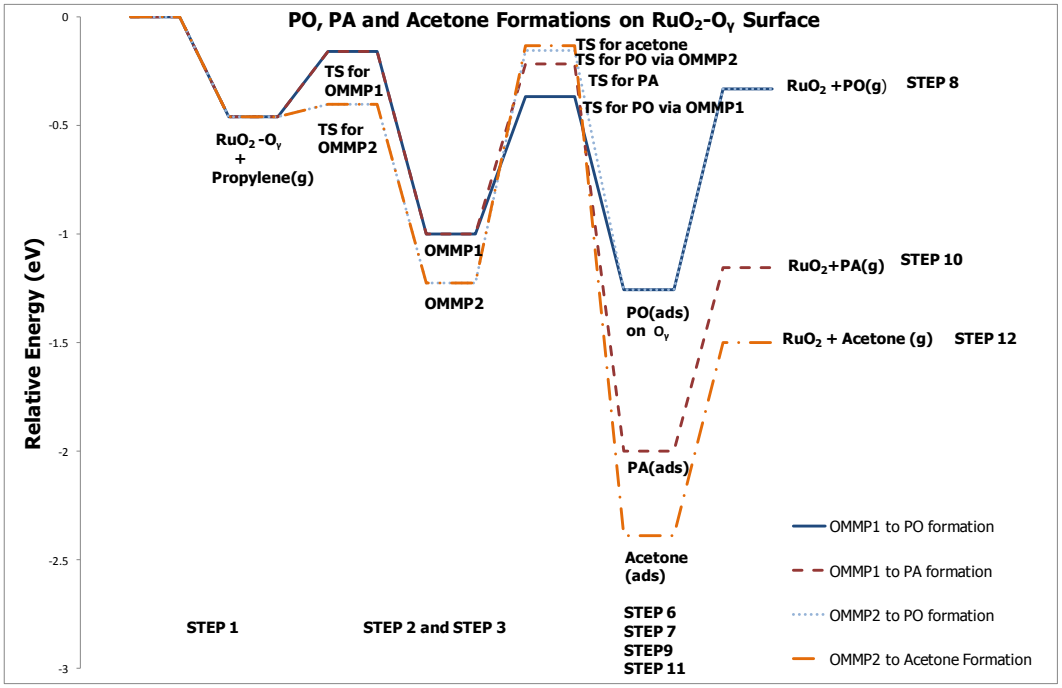

Figure 4.29: PO, PA and acetone formations on RuO_2-O_Y surface through oxametallacycle pathway

Direct PO formation on RuO_2-O_Y surface is also investigated in terms of two different paths. Figure 4.30 and 4.31 shows initial, transition state and final geometries of these direct pathways.

Propylene adsorption geometry where it is placed on top of O_Y species on the RuO_2-O_Y surface is given in Figure 4.31 (a). It further approaches to O_Y species at the transition state structure as given in Figure 4.31 (b). Following the transition state geometry, PO formation on RuO_2-O_Y surface with the insertion of O_Y can be seen in Figure 4.31 (c). The corresponding reaction is exothermic (-1.20 eV) and it requires almost no activation barrier (0.09 eV).

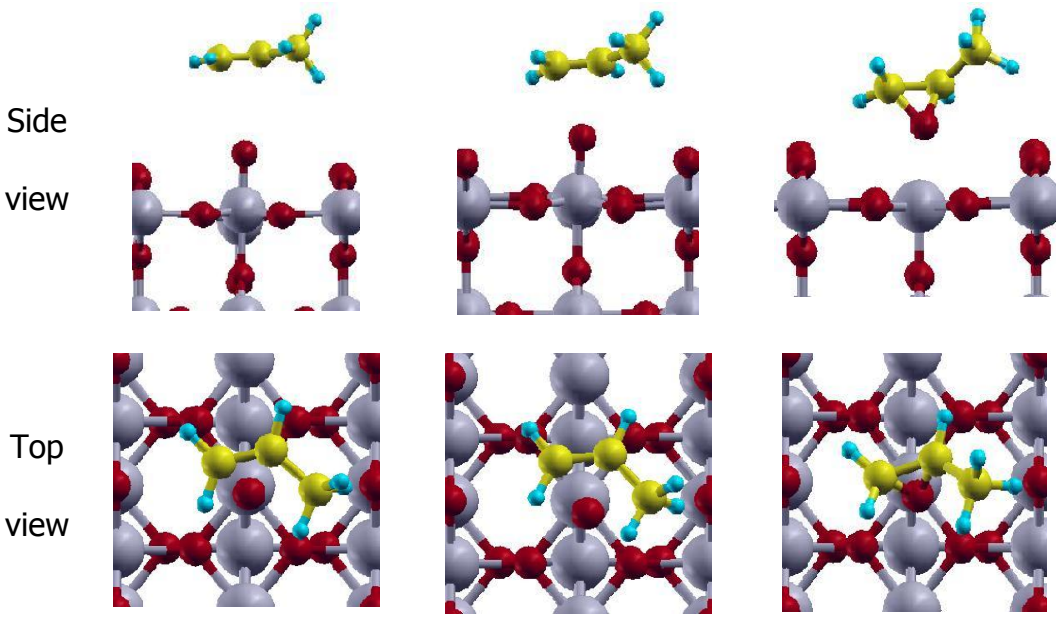

(a) Propylene Adsorption STEP 1 (b) Transition state (c) PO STEP 6

Figure 4.30: Initial, transition state and final geometries of PO formation directly from propylene adsorption on RuO_2-O_Y surface via O_Y species

Propylene adsorption geometry given in Figure 4.31 (b) is different from the propylene adsorption geometry given in Figure 4.30 (a). In the case of propylene adsorption geometry in Figure 4.31 (a), propylene is placed on top of O_{br} species. Following the approximate transition state geometry shown in Figure 4.31 (b) with activation barrier of 1.49 eV, O_{br} is placed into the propylene to form propylene oxide as given in Figure 4.31 (c). Relative energy of the direct PO formation via Obr is calculated to be -0.09 eV.

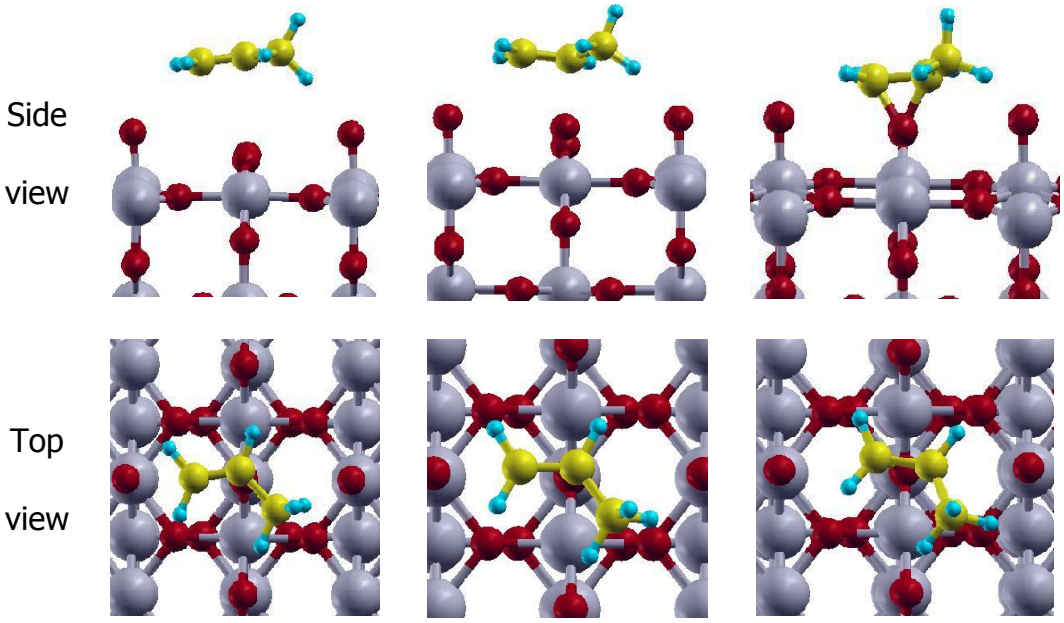

(a) Propylene Adsorption STEP 1

(b) Approximate Transition state

(c) PO STEP 6

Figure 4.31: Initial, approximate transition state and final geometries of PO formation directly from propylene adsorption on RuO_2-O_γ surface via O_{br} species

Firstly, since the aim is to see the activity of O_γ species, direct PO formation via O_γ species is analyzed where propylene approaches O_γ species and with activation of the double bond between C1 and C2, PO is produced.

Other direct path is to see the effect of O_γ species on the activity of O_{br} species. When O_γ species is present on Ru_{cus}, propylene adsorption on O_{br} species is observed for formation of PO by insertion of O_{br} between C1 and C2 of propylene. These two direct pathways and their activation barriers are shown in Figure 4.32. It is certain that PO formation via O_γ is far easier than

PO formation via O_{br}. As a matter of fact, this result is consistent with the consequence of binding energy comparison of two oxygen species in Table 4.1. Weakly bound oxygen is more active than strongly bound oxygen.

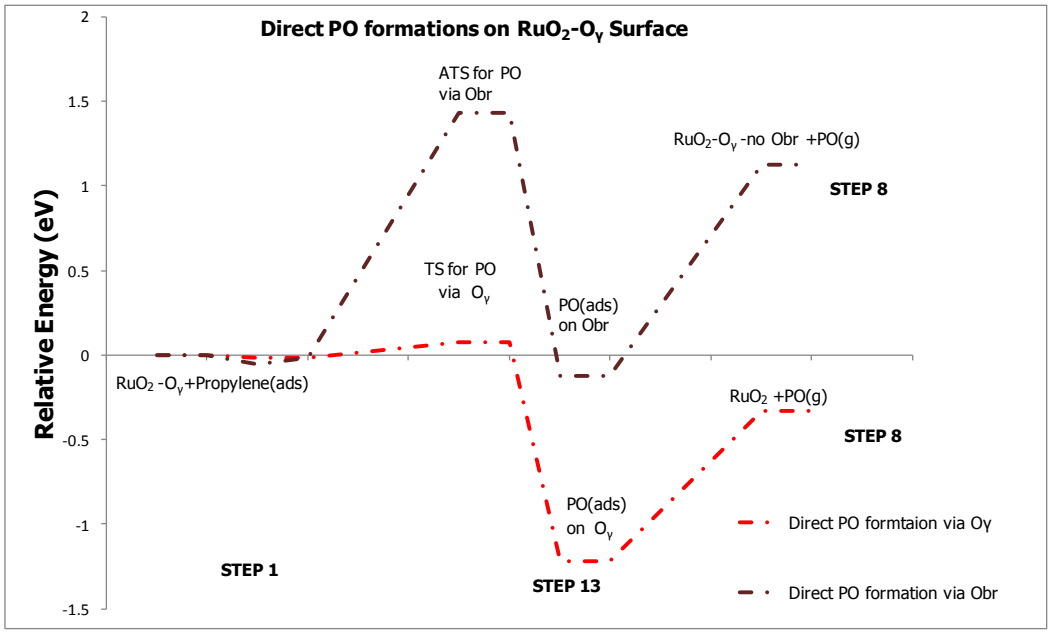

Figure 4.32: Direct PO formations on RuO_2-O_γ surface via O_γ and O_{br}

4.3. Comparison of Activation Barrier Analysis for Each Reaction

Activation barriers for each reaction investigated throughout the study on $Cu_2O(001)$, $RuO_2(110)$ and RuO_2-$O_\gamma(110)$ catalytic metal oxide surfaces are summarized in Table 4.2.

$Cu_2O(001)$ surface is found to be active for both surface intermediate OMMP2 formation and allylic hydrogen stripping since both of the reactions are exothermic steps without activation barriers. However, knowing the fact that AHS is more exothermic step in the mechanism, the reaction mechanism

is to favor the corresponding minimum energy pathway. So that the channel for the formation of acrolein opens and this study also presents the activation barrier result (0.92 eV) for the final product as acrolein. When the mechanism toward OMMP2 is favored, both of the products which are acetone and propylene oxide are to be produced on $Cu_2O(001)$ catalytic surface.

$RuO_2(110)$ surface has been found to exhibit formation of surface intermediate whereas it has lower tendency to present any final product after the surface intermediate. PO, PA and acetone formations all have high activation barrier values (1.47, 1.24 and 1.89 eV respectively).

Among all the values calculated as the results of activation barrier analysis, direct PO formation on RuO_2-O_Y surface without formation of any surface intermediate is found to have the best result that can achieve PO as the desired product. It has almost no barrier, 0.09 eV. Also formation of OMMP2 surface intermediate (with almost no activation barrier value, 0.05 eV) on RuO_2-O_Y (110) surface is highly probable to result in formation of PO (with activation barrier value of 1.07 eV). However, in this case, formation of acetone has almost similar possibility to form, as the product of the competing reaction pathway with activation barrier value of 1.09 eV. Formation of OMMP1 surface intermediate also results in both PO and PA formations at same levels of selectivity, since activation barriers for both are 0.63 eV and 0.78 eV respectively.

Table 4.2: Activation barriers for each reaction in propylene epoxidation mechanism

For	Cu_2O (001) Surface	RuO_2 (110) Surface	RuO_2-O_γ (110) Surface
OMMP1	-	0.62	0.30
OMMP2	0.00	0.19	0.05
AHS	0.00	0.34	0.61
OMMP1 to PO	-	1.47	0.63
OMMP2 to PO	0.77	1.64	1.07
OMMP1 to PA	-	1.24	0.78
OMMP2 to Acetone	0.59	1.89	1.09
Acrolein Formation	0.92	-	-
Direct PO via Obr	-	0.81	1.49
Direct PO via Oγ	-	-	0.09

Indeed activation barrier of direct PO formation via O_{br} is compared in the presence of O_γ species and without presence of O_γ species. As seen in Figure 4.32, when O_γ species are not present activity of O_{br} species is higher. To put it differently, activation barrier of direct PO formation via O_{br} is lower when O_γ species are not present as seen in Table 4.2.

4.4. Bader Charge Analysis

Selectivity of ethylene oxide was compared at different oxygen coverage on supported Ag catalyst. It was found that at high coverage, selectivity of EO was found to be higher since at high coverages, oxygen was weakly adsorbed on the surface. Also when the coverage is increased, charge on the oxygen atom will decrease [4]. Binding energy of oxygen is consistent with

the finding that on RuO_2-O_Y(110) surface where oxygen coverage is higher than RuO_2(110) surface, direct propylene oxide formation is more likely to be observed when compared to allylic hydrogen stripping. However, when there is a need for comparison with another type of catalyst, which is Cu_2O(001), binding energy of oxygen does not explain the reason of inefficiency of propylene oxide formation on Cu_2O(001) when compared to allylic hydrogen stripping. Because binding energy of oxygen on Cu_2O(001) surface is calculated to be -1.86 eV which is a value in between the binding energies of O_Y (-0.89 eV) and O_{br} (-2.31 eV) species to ruthenium oxide surface.

Besides adsorption energy of oxygen, charge of the oxygen atom has influence on the selectivity [4]. Charge density analysis where the molecular systems are divided into atomic volumes has been implemented to the results of converged electronic structure calculations [50].

In order to understand the underlying effects of propylene oxide formation on the surfaces, bader charge analysis [50] for the oxygen atoms has been implemented on all the catalytic surfaces as shown in Table 4.3. Bader charge values of the oxygen species of the corresponding catalytic surfaces revealed that, O_Y species on RuO_2-O_Y(110) surface are the most electrophilic species.

Table 4.3: Bader charge of oxygen species on the catalytic surfaces

For	Bader Charge
O_{br} species on RuO_2 (110) surface	-0.8
O_Y species on RuO_2-O_Y (110) surface	-0.7
O species on Cu_2O (001) surface	-0.9

CHAPTER 5

CONCLUSIONS

The purpose of this study is to investigate propylene epoxidation catalytic reaction mechanism on catalytic metal oxide surfaces, namely $Cu_2O(001)$, $RuO_2(110)$ and RuO_2-$O_Y(110)$ catalytic surface models. DFT calculations have been performed to analyze energies of the states in the reaction profile.

Different mechanisms have been differentiated on different metal oxide catalyst surfaces. Mainly two different types of mechanisms have been investigated for propylene oxide formation on the catalytic metal oxide surfaces, which are $Cu_2O(001)$, $RuO_2(110)$ and RuO_2-$O_Y(110)$ catalytic surface models. These mechanisms can be named as surface intermediate type mechanism and direct mechanism.

5.1. Surface Intermediate Type Mechanism on $Cu_2O(001)$ Surface

Firstly, propylene oxide formation through the surface intermediates, namely oxametallacycles, is presented. OMMP1 surface intermediate does not form on $Cu_2O(001)$ surface due to the position of allylic group of propylene towards the highly active surface oxygens for allylic hydrogen stripping. Formations of OMMP2 surface intermediate and the products, which are acetone and propylene oxide, are demonstrated in the context of surface intermediate type mechanism.

5.2. Direct Mechanism on $Cu_2O(001)$ Surface

Direct mechanism which is formation of propylene oxide without any surface intermediates is observed on all the catalytic surfaces. Direct propylene oxide formation is hindered on $Cu_2O(001)$ surface. Instead of direct propylene oxide formation, $Cu_2O(001)$ surface favors surface intermediate (OMMP2) formation or more actively favors stripping of allylic hydrogens.

5.3. Formation of Acrolein on $Cu_2O(001)$ Surface

Besides formation of propylene oxide, further reaction of allyl group on $Cu_2O(001)$ surface is also questioned for the analysis of acrolein formation. Because $Cu_2O(001)$ surface exhibit no activation barrier for both hydrogen stripping and oxametallacycle formation. Most importantly, hydrogen stripping, which results in allyl radical formation, is a highly exothermic reaction that is observed spontaneously on $Cu_2O(001)$. As far as the reactivity of the radicals is concerned, following the formation of allyl radical, analysis of stripping of the second hydrogen revealed the mechanism for acrolein formation on $Cu_2O(001)$ surface. Consequently, $Cu_2O(001)$ tends to show lower selectivity towards propylene oxide formation when compared with acrolein formation.

5.4. Surface Intermediate Type Mechanism on $RuO_2(110)$ and RuO_2-$O_Y(110)$ Surfaces

Both OMMP1 and OMMP2 surface intermediates are modeled successfully on $RuO_2(110)$ and RuO_2-$O_Y(110)$ catalytic surfaces. Surface intermediate type mechanism revealed that these structures are difficult to form further products, PO, PA and acetone, on $RuO_2(110)$ surface due to the result of

high activation barriers that have been calculated. On the contrary, RuO_2-O_Y(110) catalytic surface is found to be much more suitable on formation of corresponding products, PO, PA and acetone, upon formation of surface intermediates. The difference can be explained by different types of oxygen atoms that are included in formation of surface intermediates. In other words, on RuO_2(110) surface, O_{br} atom is included in the oxametallic cycle of surface intermediate, whereas on RuO_2-O_Y(110) surface O_Y atom is the responsible oxygen species that has been investigated for formation of oxametallacycles.

5.5. Direct Mechanism on RuO_2(110) and RuO_2-O_Y(110) Surfaces

When compared with Cu_2O(001) surface, ruthenium oxide is different towards direct mechanism. Direct PO formation is analyzed successfully on both RuO_2(110) and RuO_2-O_Y(110) catalytic surfaces. When these different types ruthenium dioxide surfaces are compared in terms of activity for direct mechanism, it can be concluded that RuO_2-O_Y(110) catalytic surface is far more reactive than RuO_2(110) surface as a consequence of the adsorption strength of oxygen species. O_{br} species are lattice oxygens that are strongly bound to the surface whereas O_Y species are bound weaker to the surface. Therefore, removal of O_Y species is more easily removed from the surface by propylene to form propylene oxide.

5.6. Final Remarks

RuO_2(110) surface is proven to be ineffective for the formation of PO. Moreover, formation of PA and acetone are not favored on RuO_2(110) surface due to high activation barriers. In order to be efficient catalyst for propylene epoxidation, RuO_2(110) catalyst is to be used after the pre-

treatment of the surface with oxygen until the formation of O_Y species on top of Ru_{cus} species. However pre-treatment should be in such a level that does not cover the entire $RuO_2(110)$ surface when propylene oxide formation through intermediate type mechanism is taken into consideration. This is due to the structural need of the oxametallacycle intermediate for a surface metal atom that is not covered by any other atomic structure. Furthermore, as explained previously, direct mechanism for formation of propylene oxide is found much more favorable on RuO_2-$O_Y(110)$ catalytic surface. To be brief, before being used as a propylene oxide catalyst, $RuO_2(110)$ surface requires pre-exposure of oxygen for achieving O_Y species bound to the surface.

The results of all the energy profile investigation revealed the differences of the catalytic surfaces towards propylene epoxidation mechanism. When compared with both $RuO_2(110)$ and RuO_2-$O_Y(110)$ catalytic surfaces, $Cu_2O(001)$ surface is mainly prone to strip allylic hydrogens which has a blocking effect on formation of propylene oxide. Subsequently, RuO_2-$O_Y(110)$ catalytic surface is found to favor propylene oxide more than any other surfaces. Underlying effect of all these implications are demonstrated in the analysis of bader charge of the oxygen species on the catalytic surfaces. As the oxygen species on the catalytic surface becomes more electrophilic, formation of propylene oxide is favored most as has been noted for RuO_2-$O_Y(110)$ catalytic surface.

REFERENCES

1.Oyama, S.T., Mechanisms in homogeneous and heterogeneous epoxidation catalysis [electronic resource] / edited by S. Ted Oyama. 2008: Amsterdam ; Boston : Elsevier, 2008.1st ed.

2.Nijhuis, T.A., Makkee, M., Moulijn, J.A., Weckhuysen, B.M., The Production of Propene Oxide: Catalytic Processes and Recent Developments. Industrial & Engineering Chemistry Research, 2006. **45**(10): p. 3447-3459.

3.Santen, R.A., Neurock, M., Molecular heterogeneous catalysis: a conceptual and computational approach. 2006: Wiley-VCH.

4.Santen, R.A, Leuwen, P.W.N.M., Moulijn, J.A., Averill, B.A., Catalysis: An Integrated Approach Second, Revised and Enlarged Edition. 2 ed. Studies in Surface Science and Catalysis. Vol. 123. 1999.

5.Bligaard, T. and Nørskov,J.K., Chapter 4 - Heterogeneous catalysis, in Chemical Bonding at Surfaces and Interfaces. 2008, Elsevier: Amsterdam. p. 255-321.

6.Thomas, J.M. and Thomas, W.J., Principles and practice of heterogeneous catalysis. 1997: VCH.

7.Santen, R.A. and Sautet,P., Computational methods in catalysis and materials science: an introduction for scientists and engineers. 2009: Wiley-VCH.

8.Vajda, S., Lee S., Sell, K., Barke I., Kleibert, A., Oeynhausen, V., Meiwes-Broer, K., Rodriguez, A.F., Elam, J.W., Pellin, M.M., Lee, B., Seifert, S., Winans, R.E., Combined temperature-programmed reaction and in situ x-ray scattering studies of size-selected silver clusters under realistic reaction conditions in the epoxidation of propene. Journal of Chemical Physics, 2009. **131**(12).

9.Le, Y., Mehmood, F., Lee, S., Greeley, J., Lee, B., Seifert, S., Winans, R.E., Elam, J.W., Meyer, R.J., Teschner, D., Schlögl, R., Pellin, M.J., Curtiss, L.E., Vajda, S., Increased silver activity for direct propylene epoxidation via subnanometer size effects. Science, 2010. **328**(5975): p. 224-228.

10.Molina, L.M., Lee,S., Sell, K., Barcara, G., Fortunelli, A., Lee, B., Seifert, S., Winans, R.E., Elam, J.W., Pellin, M.J., Barke, I., Oeynhausen, V., Lei, Y., Meyer, R.J., Alonso, J.A.,Rodriguez, A.F., Kleibert, A., Giorgio, S., Henry, C.R, Meiswes-Broer, K.,Jajda, S., Size-dependent selectivity and activity of silver nanoclusters in the partial oxidation of propylene to propylene oxide and acrolein: A joint experimental and theoretical study. Catalysis Today, 2011. **160**(1): p. 116-130.

11.Deng, X., Min, B. K., Liu, X., Friend C.M., Partial Oxidation of Propene on Oxygen-Covered Au(111). The Journal of Physical Chemistry B, 2006. **110**(32): p. 15982-15987.

12.Roldan, A., Torres, D., Ricart, J. M., Illas, F., On the effectiveness of partial oxidation of propylene by gold: A density functional theory study. Journal of Molecular Catalysis A: Chemical, 2009. **306**(1-2): p. 6-10.

13.Kobayashi, H.,Shimodaira, Y., Density functional study of propylene oxidation on Ag and Au surfaces. Comparison to ethylene oxidation. Journal of Molecular Structure: THEOCHEM, 2006. **762**(1-3): p. 57-67.

14.Kahn, M., Seubsai, A., Onal, I., Senkan, S., New catalytic materials for the direct epoxidation of propylene by oxygen: Application of high-throughput pulsed laser ablation. Topics in Catalysis, 2010. **53**(1-2): p. 86-91.

15.Vaughan, O.P.H., Kyriakou, G., Macleod, N., Tikhov, M., Lambert, R. M., Copper as a selective catalyst for the epoxidation of propene. Journal of Catalysis, 2005. **236**(2): p. 401-404.

16.Su, W., Wang, S., Ying, P., Feng, Z., Li, C., A molecular insight into propylene epoxidation on Cu/SiO_2 catalysts using O_2 as oxidant. Journal of Catalysis, 2009. **268**(1): p. 165-174.

17.Monnier, J.R., Hartley, G.W., Comparison of Cu and Ag Catalysts for Epoxidation of Higher Olefins. Journal of Catalysis, 2001. **203**(1): p. 253-256.
18.Zhu, W., Zhang, Q., Wang, Y., Cu(I)-catalyzed epoxidation of propylene by molecular oxygen. Journal of Physical Chemistry C, 2008. **112**(20): p. 7731-7734.
19.Onal, I., Duzenli, D., Seubsai, A., Kahn, M., Seker, E., Senkan, S., Propylene epoxidation: High-throughput screening of supported metal catalysts combinatorially prepared by rapid sol-gel method. Topics in Catalysis, 2010. **53**(1-2): p. 92-99.
20.Lu, J., Luo, M., Lei, H., Bao, X., Li, C., Epoxidation of Propylene on NaCl-Modified VCe1-x Cux Oxide Catalysts with Direct Molecular Oxygen as the Oxidant. Journal of Catalysis, 2002. **211**(2): p. 552-555.
21.Reitz, J.B., Solomon, E.I., Propylene oxidation on copper oxide surfaces: Electronic and geometric contributions to reactivity and selectivity. Journal of the American Chemical Society, 1998. **120**(44): p. 11467-11478.
22.Chu, H., Yang, L., Zhang, Q., Wang, Y., Copper-catalyzed propylene epoxidation by molecular oxygen: Superior catalytic performances of halogen-free K+-modified CuOx/SBA-15. Journal of Catalysis, 2006. **241**(1): p. 225-228.
23.Wang, Y., Chu, H., Zhu, W., Zhang, Q., Copper-based efficient catalysts for propylene epoxidation by molecular oxygen. Catalysis Today, 2008. **131**(1-4): p. 496-504.
24.Yang, L., He, J., Zhang, Q., Wang, Y., Copper-catalyzed propylene epoxidation by oxygen: Significant promoting effect of vanadium on unsupported copper catalyst. Journal of Catalysis, 2010. **276**(1): p. 76-84.
25.López, N., Novell-Leruth, G., Rules for selectivity in oxidation processes on RuO_2(110). Physical Chemistry Chemical Physics, 2010. **12**(38): p. 12217-12222.

26.Paulus, U.A., Wang, Y., Bonzel, H.P., Jacobi, K., Ertl, G., Adsorption and interaction of ethylene on RuO2(110) surfaces. Journal of Physical Chemistry B, 2005. **109**(6): p. 2139-2148.

27.Seubsai, A., Kahn, M., Senkan, S., New Catalytic Materials for the Direct Epoxidation of Propylene by Molecular Oxygen. ChemCatChem, 2011. **3**(1): p. 174-179.

28.Kizilkaya, A.C., Senkan, S., Onal,I., Investigation of ruthenium-copper bimetallic catalysts for direct epoxidation of propylene: A DFT study. Journal of Molecular Catalysis A: Chemical, 2010. **330**(1-2): p. 107-111.

29.Linic, S., Barteau, M.A., Formation of a Stable Surface Oxametallacycle that Produces Ethylene Oxide. Journal of the American Chemical Society, 2001. **124**(2): p. 310-317.

30.Özbek, M.O., I. Önal, van Santen, R.A., Ethylene Epoxidation Catalyzed by Silver Oxide. ChemCatChem, 2011. **3**(1): p. 150-153.

31.Torres, D., Lopez, N., Illas, F., Lambert, R.M., Low-basicity oxygen atoms: A key in the search for propylene epoxidation catalysts. Angewandte Chemie - International Edition, 2007. **46**(12): p. 2055-2058.

32.Lambert, R.M., Williams, F.J., Cropley, R.L., Palermo, A., Heterogeneous alkene epoxidation: Past, present and future. Journal of Molecular Catalysis A: Chemical, 2005. **228**: p. 27-33.

33.Williams, F.J., Cropley, R.L., Vaughan, O.P.H, Urquhart, A.J., Tikhov, M.S., Kolczewvski, C., Hermann, K., Lambert, R.M., Critical influence of adsorption geometry in the heterogeneous epoxidation of "allylic" alkenes: Structure and reactivity of three phenylpropene isomers on Cu(111). Journal of the American Chemical Society, 2005. **127**(48): p. 17007-17011.

34.Cropley, R.L., Williams, F.J., Urquhart, A.J., Vaughan, O.P.H., Tikhov, M.S., Lambert, R.M., Efficient epoxidation of a terminal alkene containing allylic hydrogen atoms: trans-methylstyrene on Cu{111}. Journal of the American Chemical Society, 2005. **127**(16): p. 6069-6076.

35.Kresse, G., Furthmüller, J., Efficiency of ab-initio total energy calculations for metals and semiconductors using a plane-wave basis set. Computational Materials Science, 1996. **6**(1): p. 15-50.
36.Kresse, G., Furthmüller, J., Efficient iterative schemes for ab initio total-energy calculations using a plane-wave basis set. Physical Review B, 1996. **54**(16): p. 11169.
37.Perdew, J.P. and Y. Wang, Accurate and simple analytic representation of the electron-gas correlation energy. Physical Review B, 1992. **45**(23): p. 13244.
38.Perdew, J.P., Chevary, J.A., Vosko, S.H., Jackson, K.A., Pederson, M.R., Singh, D.,J., Fiolhais, C., Atoms, molecules, solids, and surfaces: Applications of the generalized gradient approximation for exchange and correlation. Physical Review B, 1992. **46**(11): p. 6671.
39.Blöchl, P.E., Projector augmented-wave method. Physical Review B, 1994. **50**(24): p. 17953.
40.Monkhorst, H.J., Pack, J.D., Special points for Brillouin-zone integrations. Physical Review B, 1976. **13**(12): p. 5188.
41.Henkelman, G., Uberuaga, B.P., Jónsson, H., Climbing image nudged elastic band method for finding saddle points and minimum energy paths. Journal of Chemical Physics, 2000. **113**(22): p. 9901-9904.
42.Schulz, K.H., Cox, D.F., Photoemission and low-energy-electron-diffraction study of clean and oxygen-dosed Cu_2O (111) and (100) surfaces. Physical Review B, 1991. **43**(2): p. 1610.
43.Le, D.,Stolbov, S., Rahman, T.S., Reactivity of the Cu_2O(1 0 0) surface: Insights from first principles calculations. Surface Science, 2009. **603**(10-12): p. 1637-1645.
44.Kim, Y.D., Seitsonen, A.P., Wendt, S., Wang, J.F., Jacobi, K., Over, H., Ertl, G., Characterization of various oxygen species on an oxide surface: RuO_2(110). Journal of Physical Chemistry B, 2001. **105**(18): p. 3752-3758.

45.Wang, Y., Jacobi, K., Schöne, W.D., Ertl, G., Catalytic oxidation of ammonia on RuO_2(110) surfaces: Mechanism and selectivity. Journal of Physical Chemistry B, 2005. **109**(16): p. 7883-7893.

46.Wang, H., Schneider, W.F., Adsorption and reactions of NO_x on RuO_2(110). Catalysis Today, 2011. **165** (1) : p. 49-55

47.Over, H., Kim, Y.D., Seitsonen, A.P., Wendt, S., Lundgren, E., Schmid, M., Varga, P., Morgante, A., Ertl, G., Atomic-scale structure and catalytic reactivity of the RuO_2(110) surface. Science, 2000. **287**(5457): p. 1474-1476.

48.Wang, H., Schneider, W.F., Schmidt, D., Intermediates and spectators in O_2 dissociation at the RuO_2(110) surface. Journal of Physical Chemistry C, 2009. **113**(34): p. 15266-15273.

49.Fellah, M., Onal, I., Epoxidation of Propylene on a [$Ag_{14}O_9$] Cluster Representing Ag_2O (001) Surface: A Density Functional Theory Study. Catalysis Letters, 2012. **142**(1): p. 22-31.

50.Tang, W.,Sanville, E., Henkelman, G., A grid-based Bader analysis algorithm without lattice bias. Journal of Physics: Condensed Matter, 2009. **21**(8): p. 084204.

APPENDIX A

SAMPLE INPUT FILES FOR VASP CODE

A.1. Bulk Structure Optimization

In order to model bulk ruthenium dioxide structure, POSCAR file is created initially that describes the position of the atoms that represent bulk structure. In other words, POSCAR is defines the geometry of the input. Bulk structure is so critical that it has to define all the volume of elements in all the directions. POSCAR file for the bulk structure optimization is shown as the following:

```
Ru O
1.00000000000000
     4.5455759997659433    0.0000000000000000    0.0000000000000000
     0.0000000000000000    4.5455759997659433    0.0000000000000000
     0.0000000000000000    0.0000000000000000    3.1371691611788322
   2   4
Selective dynamics
Direct
0.0000000000000000  0.0000000000000000  0.000000000000000   T   T   T
0.5000000000000000  0.5000000000000000  0.500000000000000   T   T   T
0.3058936336535893  0.3058936336535893  0.000000000000000   T   T   T
0.6941063663464178  0.6941063663464178  0.000000000000000   T   T   T
0.8058936336535822  0.1941063663464107  0.500000000000000   T   T   T
0.1941063663464107  0.8058936336535822  0.500000000000000   T   T   T
```

KPOINTS is the indicator of the number of k-points that are used for defining Brillouin zone. For bulk structure model, it is important to use high value of K-points in order to get a well optimized structure.

```
K-Points
 0
Monkhorst Pack
 19  19  19
 0  0  0
```

INCAR is the indicator of the optimization algorithm. It includes several keywords that define all the calculation parameters. INCAR that has been used for the optimization of bulk structure is:

```
SYSTEM = Ru O
ISTART = 0
PREC   = HIGH
ISIF   = 3
IBRION = 2; !NFREE = 20;
NSW    = 150
LREAL  = .FALSE.
ISMEAR = 0; SIGMA = 0.01
ENCUT = 500
!IALGO = 48
EDIFFG = 1e-3
LWAVE = .FALSE.
!IDIPOLE = 3
!LDIPOLE = .TRUE.
LCHARGE = .FALSE.
```

POTCAR file that has been defined specific to the catalytic reactive medium that includes potential of each elements in the system. In other words, POTCAR includes the pseudopotentials. After creating POTCAR file for the system by combining POTCAR for each atom, it is controlled as following

screen. It should be combined in the order of the atoms defined in the geometrical input file, POSCAR.

```
PAW_GGA Ru 03Mar1998
   TITEL  = PAW_GGA Ru 03Mar1998
   LPAW   =       T    paw PP
 PAW radial sets
 PAW_GGA O 05Jan2001
   TITEL  = PAW_GGA O 05Jan2001
   LPAW   =       T    paw PP
 PAW radial sets
```

After the calculation with the corresponding parameters, each atom where the positions of each are indicated in POSCAR geometry is optimized. Result of the optimized geometry of the bulk structure can be seen in CONTCAR file.

```
Ru O
   1.00000000000000
     4.5455759997659433    0.0000000000000000    0.0000000000000000
     0.0000000000000000    4.5455759997659433    0.0000000000000000
     0.0000000000000000    0.0000000000000000    3.1371691611788322
   2   4
Selective dynamics
Direct
  0.0000000000000000  0.0000000000000000  0.00000000000000   T   T   T
  0.5000000000000000  0.5000000000000000  0.50000000000000   T   T   T
  0.3058936336535893  0.3058936336535893  0.00000000000000   T   T   T
  0.6941063663464178  0.6941063663464178  0.00000000000000   T   T   T
  0.8058936336535822  0.1941063663464107  0.50000000000000   T   T   T
  0.1941063663464107  0.8058936336535822  0.50000000000000   T   T   T
```

A.2. Optimization of Slab

Sample input geometry for optimization of a slab and also the reactant/product on the slab is shown as the following POSCAR file:

Ru O C H
1.00000000000000
6.2743000000000002 0.0000000000000000 0.0000000000000000
0.0000000000000000 6.4283999999999999 0.0000000000000000
0.0000000000000000 0.0000000000000000 27.1523000000000003
16 33 3 6
Selective dynamics
Direct
0.000000000000000 0.000000000000000 0.0462100000000021 F F F
0.500000000000000 0.000000000000000 0.0462100000000021 F F F
0.250000000000000 0.500000000000000 0.0462100000000021 F F F
0.750000000000000 0.500000000000000 0.0462100000000021 F F F
0.999335657018143 0.499515598368052 0.3942383759532649 T T T
0.499708863102112 0.499357560007849 0.3977626337415179 T T T
0.244509811090799 0.000515733882863 0.4014106958185787 T T T
0.755926675972093 0.000166198246080 0.4016680782105347 T T T
-0.000007036025051 0.499814206817129 0.1640766117626817 T T T
0.500015584293514 0.499885218599326 0.1638393867878022 T T T
0.250067358830509 0.999690517387006 0.1623899259277634 T T T
0.749950392618535 0.999672640181979 0.1623868343403448 T T T
0.251868196495855 0.499575163643396 0.2810249157353217 T T T
0.748377626536486 0.500005104043828 0.2809318942824846 T T T
0.000034974255783 0.999871686609518 0.2807252386518233 T T T
0.500098519649951 8 0.000008316480 30 0.2815294178969380 T T T
0.000000000000000 0.500000000000000 0.0000000000000000 F F F
0.500000000000000 0.500000000000000 0.0000000000000000 F F F
0.250000000000000 0.195199999999999 0.0462100000000021 F F F
0.750000000000000 0.195199999999999 0.0462100000000021 F F F
0.250000000000000 0.804800000000000 0.0462100000000021 F F F
0.750000000000000 0.804800000000000 0.0462100000000021 F F F
0.999596959573265 0 0.500145455952410 0.0928622509063364 T T T
0.499592572180164 1 0.500142677042200 0.0928249651945590 T T T
0.000001423165508 7 0.998658429112190 0.1171135308365290 T T T
0.500008754963672 5 0.998716535638570 0.1171354256482679 T T T
0.249955088855370 3 0.305785762471600 0.1633719122694310 T T T
0.750026888873458 9 0.305781991700340 0.1633734829773542 T T T
0.249985980629532 6 0.693857730207600 0.1642969790046993 T T T
0.749992809405702 1 0.693847362737350 0.1643006759238301 T T T
0.000022586423503 3 0.000126092184860 0.2085047773452337 T T T
0.499993104302712 7 0.001220151766130 0.2086381807914658 T T T
0.000123437083284 8 0.499801299712120 0.2356753128412196 T T T
0.500010076114724 7 0.499800598736300 0.2355714128158243 T T T
0.250621192951833 2 0.806004963127410 0.2804016766889104 T T T

0.7496160012645323	0.80616194550765	0.2803580187376891	T	T	T
0.2504196104017868	0.19376568554584	0.2803810807326815	T	T	T
0.7496344174881627	0.19386282853533	0.2803702038230802	T	T	T
0.0000240712950793	0.50008649761739	0.3248607588063898	T	T	T
0.5002919019456835	0.50032109258159	0.3269223656369060	T	T	T
0.0000376121168385	0.99997700349923	0.3531391743991744	T	T	T
0.5000991823303557	0.00003017975139	0.3535756247612367	T	T	T
0.2488015128878694	0.69197645235779	0.4001224532159391	T	T	T
0.7511289844991177	0.69198851298443	0.4002571605732537	T	T	T
0.2483843938097556	0.30778158850361	0.3998180043661815	T	T	T
0.7512176751333692	0.30752948205791	0.3999626518953356	T	T	T
0.0005720211006923	0.99965119036278	0.4471078076438144	T	T	T
0.4999609301766547	0.99894977497865	0.4406318274998551	T	T	T
0.4859925753564943	0.45828808318097	0.4774091492281756	T	T	T
0.2936988765576267	0.49195763976728	0.5066016717982248	T	T	T
0.6272448895145948	0.50696297768684	0.5628911901796463	T	T	T
0.4948521196550499	0.59233309752238	0.5214837915381921	T	T	T
0.7958540325965026	0.54794564287580	0.5584151602907463	T	T	T
0.5720601154064424	0.57314010503362	0.5980012747844533	T	T	T
0.5132675214488305	0.75653379841618	0.5117891185610455	T	T	T
0.6125390415108354	0.33697400602545	0.5647127900223656	T	T	T
0.2384473935147015	0.35075189804833	0.5249129351616725	T	T	T
0.1730583972361706	0.58830800117811	0.4886519944520277	T	T	T

KPOINTS of a slab optimization is given below:

```
K-Points
 0
Monkhorst Pack
 4  4  1
 0  0  0
```

INCAR file that includes the keyword parameters for the optimization of the slab or the corresponding reactant/product on the slab is shown as:

```
EDIFFG = -0.015
IBRION = 2
!POTIM = 0.2;
!NFREE  = 20
```

```
ISMEAR = 0; SIGMA = 0.01;
LREAL = Auto
ENCUT  = 500
IDIPOL = 3
LDIPOL = .TRUE.
NSW    = 300
ALGO=FAST
```

POTCAR file including the pseudopotentials of the elements present in the system to be optimized is checked and the screen is given below as:

```
PAW_GGA Ru 03Mar1998
  TITEL  = PAW_GGA Ru 03Mar1998
  LPAW   =       T    paw PP
PAW radial sets
PAW_GGA O 05Jan2001
  TITEL  = PAW_GGA O 05Jan2001
  LPAW   =       T    paw PP
PAW radial sets
PAW_GGA C 05Jan2001
  TITEL  = PAW_GGA C 05Jan2001
  LPAW   =       T    paw PP
PAW radial sets
PAW_GGA H 07Jul1998
  TITEL  = PAW_GGA H 07Jul1998
  LPAW   =       T    paw PP
PAW radial sets
```

After the use of all required parameters, CONTCAR file shows the optimized slab, on which reactant/surface intermediate/product is placed. CONTCAR file indicating the position of each atom of the calculated system is as follows:

```
Ru O C H
   1.00000000000000
     6.2743000000000002    0.0000000000000000    0.0000000000000000
     0.0000000000000000    6.4283999999999999    0.0000000000000000
     0.0000000000000000    0.0000000000000000   27.1523000000000003
  16  33   3   6
Selective dynamics
```

Direct

0.0000000000000000	0.00000000000000	0.0462100000000021	F	F	F
0.5000000000000000	0.00000000000000	0.0462100000000021	F	F	F
0.2500000000000000	0.50000000000000	0.0462100000000021	F	F	F
0.7500000000000000	0.50000000000000	0.0462100000000021	F	F	F
0.9994360023820079	0.49934121024824	0.3942623780715770	T	T	T
0.4990753803697887	0.49882708482739	0.3978659783032188	T	T	T
0.2442951974765648	0.00043564596909	0.4014851701642173	T	T	T
0.7557542037556322	-0.00013093578199	0.4016302287697845	T	T	T
-0.0000331028443866	0.49963889516105	0.1640063078298052	T	T	T
0.5000016632735634	0.49964648736517	0.1638164961687444	T	T	T
0.2500067724506340	-0.00057868384588	0.1623517796857095	T	T	T
0.7498686143185055	-0.00040320804251	0.1624011979128321	T	T	T
0.2517735573785109	0.49975010869640	0.2810426145389419	T	T	T
0.7482014278039526	0.50007949424252	0.2809520936927529	T	T	T
0.0000025745238289	0.99997330878553	0.2807349750740794	T	T	T
0.5000239600603875	0.00008754441268	0.2815316307115157	T	T	T
0.0000000000000000	0.50000000000000	0.0000000000000000	F	F	F
0.5000000000000000	0.50000000000000	0.0000000000000000	F	F	F
0.2500000000000000	0.19519999999999	0.0462100000000021	F	F	F
0.7500000000000000	0.19519999999999	0.0462100000000021	F	F	F
0.2500000000000000	0.80480000000000	0.0462100000000021	F	F	F
0.7500000000000000	0.80480000000000	0.0462100000000021	F	F	F
0.0003333505855719	0.50007409112188	0.0928395457338837	T	T	T
0.5004393229769919	0.50006344662945	0.0928146736852294	T	T	T
-0.0000681457117494	0.99865358592702	0.1171085712294127	T	T	T
0.4999710007816092	0.99871526340745	0.1171300827823173	T	T	T
0.2499341477473596	0.30568640212253	0.1633773662702125	T	T	T
0.7500165340287446	0.30569995033070	0.1633838362975492	T	T	T
0.2499739547421459	0.69315325327569	0.1638067833888849	T	T	T
0.7499734308396474	0.69381691069554	0.1642964711520558	T	T	T
0.0000067523845596	0.00004720536127	0.2085060272539452	T	T	T
0.4999078268459342	0.00113395978467	0.2086427072882391	T	T	T
0.0000895473670011	0.49983540135148	0.2356684117415934	T	T	T
0.4999035277246749	0.49984282327535	0.2355688338646871	T	T	T
0.2505668148782561	0.80605190466150	0.2804053430217125	T	T	T
0.7495595776956026	0.80618577260640	0.2803681203460818	T	T	T
0.2505355433420452	0.19390502061901	0.2804211786187769	T	T	T
0.7495808754664973	0.19389323243401	0.2803746553295128	T	T	T
-0.0000628116360750	0.50010854313935	0.3248720056998822	T	T	T
0.5003383020599191	0.50043630224316	0.3269701611103472	T	T	T
-0.0001192976416483	-0.00009535255967	0.3531464688886222	T	T	T
0.5000479638374042	-0.00002320735471	0.3535864607366141	T	T	T

0.2486276378668946	0.69205062550461	0.4001528863220313	T	T	T
0.7506699148022796	0.69116967714135	0.4004542855078426	T	T	T
0.2480115305088919	0.30739416088399	0.3998118642814565	T	T	T
0.7510849931235370	0.30752808229260	0.3999809481609409	T	T	T
0.0004727620880849	0.99953882254653	0.4471213683637488	T	T	T
0.4999218133384388	0.99895157477995	0.4406303759063184	T	T	T
0.4862777575769723	0.45953683674000	0.4775091390792682	T	T	T
0.3030999522790184	0.51167807852415	0.5084342088888202	T	T	T
0.6471383074070971	0.52004877409301	0.5610533287136827	T	T	T

A.3. CI-NEB Calculations

Input geometry for CI-NEB calculations consists of several geometries written in POSCAR format. They are obtained by dividing the initial and the final state into a number of images. In other words, they are images in between initial and final state to achieve the location of transition state image.

K-POINTS and POTCAR files used for CI-NEB calculations are the same as optimization of slab.

INCAR file includes the parameters used for calculation of CI-NEB. It is given as:

```
!FOR CNEB
IMAGES = 8
SPRING = -5
ICHAIN = 0
LCLIMB = .TRUE.
LTANGENTOLD = .FALSE.
LDNEB  = .FALSE.
!EDIFFG = -0.015
IBRION = 1;
POTIM = 0.2;
!NFREE  = 20
NSW    = 200
LDIPOL = .TRUE.
ISMEAR = 0; SIGMA = 0.1;
LREAL = Auto
```

```
ENCUT  = 500
IDIPOL = 3
LCHARG = .FALSE.
ALGO=FAST
```

A.4. Vibrational Frequency Analysis

Vibrational frequency analysis is applied to the transition state structure calculated after the convergence of the CI-NEB calculations. Output geometry obtained for transition state structure at the end of CI-NEB calculations is used as POSCAR file, or in other words input geometry of vibrational frequency analysis.

KPOINTS and POTCAR files are the same as the ones used for calculations of slab optimizations.

INCAR file including the calculation comments used for vibrational frequency analysis is given as:

```
PREC   = HIGH
ISYM=0
EDIFFG = -0.015
EDIFF = 1e-6
IBRION = 5; POTIM = 0.02;
!NFREE  = 20
ISMEAR = 0; SIGMA = 0.1;
LREAL = Auto
ENCUT  = 500
NSW    = 900
LDIPOL = .TRUE.
IDIPOL = 3
LCHARGE = .FALSE.
LWAVE=.FALSE.
ALGO=FAST
```

APPENDIX B

SAMPLE RELATIVE ENERGY PROFILE

CI-NEB analysis is applied to each elementary steps in the mechanism for the activation barrier analysis. Figure A.1 illustrates the sample energy profile that has been achieved at the end of the activation barrier analysis for allylic hydrogen stripping.

Profile between the initial state and final state is divided into 8 images and all energies of all the images have been calculated. Transition state is distinguished at the image indicated as number 5 in the figure.

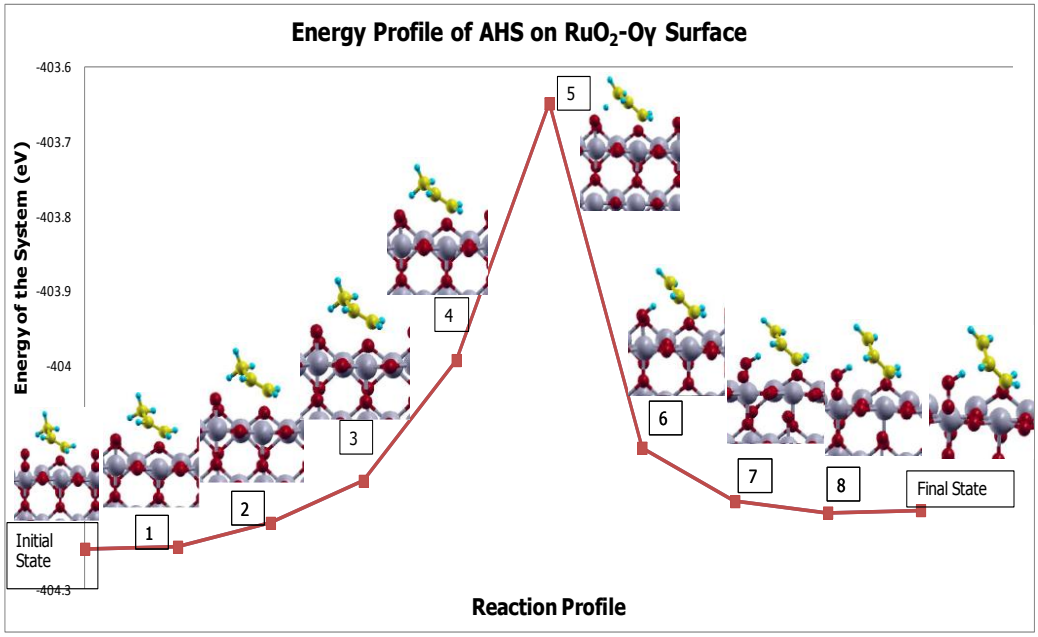

Figure A.1: Sample energy profile of AHS on RuO_2-O_γ surface